



CORSO DI DOTTORATO DI RICERCA IN SCIENZA E GESTIONE DEI CAMBIAMENTI CLIMATICI Ciclo XXXI

Tesi di Ricerca

A modelling framework for EBUS: from seasonal to decadal time scales

COORDINATORE DEL DOTTORATO:

Prof. Carlo Carraro

SUPERVISORI:

Dr. Simona Masina

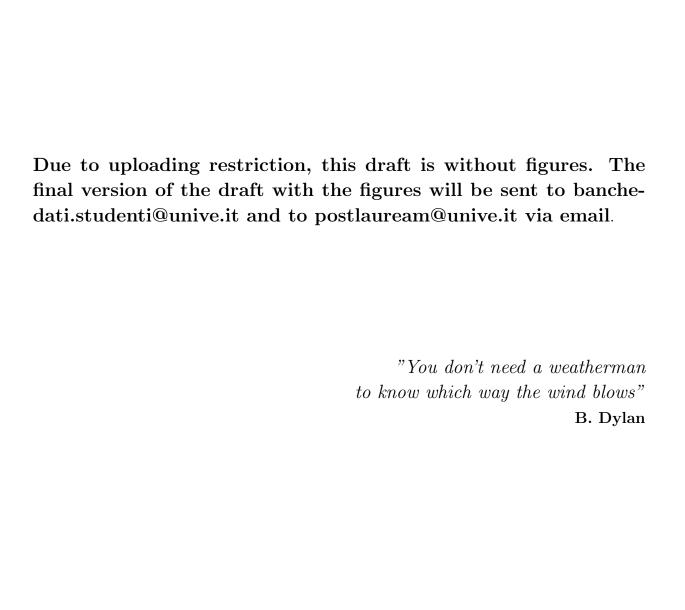
Dr. Dorotea Iovino

Dr. Andrea Storto

DOTTORANDA:

Giulia Bonino

Matricola 956212



Abstract

Along major Eastern Boundary Upwelling Systems (EBUS) local and seasonal changes in the equatorward wind stress (e.g. Ekman Upwelling) and cross-shore gradients of the wind (e.g. Ekman Pumping) are the main drivers of the three dimensional ocean circulation that controls coastal sea surface temperature (SST) and the upwelling of ocean tracers (e.g. nutrients). Through modulation of these local conditions, also climate modes seem to have an impact on upwelling, regulating the EBUS variability at interannual and decadal timescales. In light of the importance of the forcing, in a ocean modelling framework, the aims of this thesis are (1) to understand the impact of different wind structures on the dynamics of SST and upwelling and, (2) to detect and compare low-frequency variability and changes in EBUS. The analysis of available atmospheric reanalyses products, ERAInterim ($\sim 80km$ resolution) and the very recent JRA55-do-v1.1($\sim 55km$ resolution), showed important differences in the structure of the wind stress and wind stress curl along the EBUS when compared to the shorter satellite record from QuikSCAT (1999-2009, $\sim 25km$ resolution). Thus, to achieve the first objective, we performed long-term ocean hindcasts from 1985-2015 with the global ORCA025 configuration (25 km of horizontal resolution) of NEMO (version 3.6) general circulation model forced by the two reanalyses. The numerical results suggest that (1) coastal upwelling and Ekman pumping are locally forced by differences in alongshore wind stress and wind stress curl (WSC), respectively; (2) equatorward currents are intensified under enhanced wind stress condition, while poleward undercurrents respond to WSC changes; (3) SST differences are mostly related to a stronger nearshore wind stress rather than incoming heat fluxes due to enhanced vertical velocities and along-shore equatorward currents downwind (cold advection). Motivated by these results, and to investigate the low-frequency variability in a larger-scale climate prospective, we develop a new atmospheric forcing product (25 km) obtained through a statistical downscaling and merger of the high resolution QuikSCAT winds with the largescale wind structures from JRA55. The new forcing is used to force the third long-term ocean hindcast from 1958 to 2015 with an ensemble of passive tracers, which are released at the subsurface (150m-300m) at each EBUS from coast to 50 Km offshore. The statistical analysis of passive tracers concentration at surface, which represents upwelled coastal water masses, allowed us to study the large-scale drivers of upwelling variability and trends.

The simulation is found to reproduce well the seasonal cycle of upwelling intensity over all EBUS areas, with a maximum in boreal summer in the Northern Hemisphere Systems and in boreal winter in the Southern Hemisphere Systems. In all the systems, the seasonal fluctuations of the common atmospheric patterns favouring upwelling (e.g., equatorward wind/wind stress, wind stress curl and heat fluxes) drive the low-frequency modulation of the upwelling seasonal cycle. In particular, Benguela Upwelling System and Canary Upwelling System show long-term trends driven by wind forcing and stratification respectively. In addition, the statistical link between upwelling across the EBUS and large-scale climate variability modes is analysed. We performed an EOF analysis of the passive tracers concentration time series in order to evaluate EBUS shared covariability. Even though a global covariability across EBUS is not detected, at basin scale the El Ni \tilde{n} o-Southern Oscillation and its low frequency modulation exert influence on Pacific systems (e.g. California and Peru systems), while the Atlantic Meridional Oscillation (AMO) is the predominant mode over Atlantic domains (e.g. Benguela and Canary systems). Moreover, to some extent, the Northern Hemisphere domains are controlled by Meridional Modes (PMM and AMM) through the modulation of wind and SST patterns, while the Southern Hemisphere domains are influenced by Antarctica atmospheric variability, in particular by the AAO, which is affected by the strength of the circumpolar westerly flow, and can influence equatorward favorable winds.

Table of Contents

T	Intr	oduction				
	1.1	Upwelling and Eastern Boundary Upwelling Systems (EBUS)	1			
	1.2	Open Scientific Questions	3			
	1.3	Thesis objectives	4			
2	Ana	alysis of the atmospheric and surface oceanic temporal variability				
	in t	he EBUS	7			
	2.1	Introduction				
	2.2	Model Configuration and Data	8			
		2.2.1 Model description and experiments	8			
		2.2.2 Observations for validation	9			
	2.3	Results	10			
		2.3.1 Wind Forcing variability on EBUS	10			
		2.3.2 Ocean dynamical response	13			
	2.4	Discussion and Conclusion	15			
3	$\mathbf{E}\mathbf{B}^{\dagger}$	US response to different atmospheric forcing in a global eddy-permittin	\mathbf{g}			
	oce	an model	19			
	3.1	Introduction	19			
	3.2	Model Configuration and Data				
	3.3	Results	21			
		3.3.1 Wind Forcing analysis in the EBUS	22			
		3.3.2 Coastal Currents in the EBUS	23			
		3.3.3 Sea Surface Temperature analysis in the EBUS	26			
	3.4	Discussion and Concluding remarks	28			
4	Inte	erannual to decadal Climate Variability within and across the major				
	Eas	tern Boundary Upwelling Systems	33			
	4.1	Introduction	33			
	4.2	Data and methods	36			
		4.2.1 Ocean model setup	36			
		4.2.2 Indices and observation	39			

	4.3	Result	S	41	
		4.3.1	Model Validation	41	
		4.3.2	Upwelling Seasonal Cycle	42	
		4.3.3	Drivers and trends of low frequency modulation of upwelling \dots .	43	
4.4 Correlation with climate modes and Coherent low-frequency variability					
		EBUS		44	
		4.4.1	Correlation with climate modes	45	
		4.4.2	Shared climate variability across EBUS	47	
	4.5	Discus	ssion and conclusions	49	
5	Sun	nmary	and Conclusions	55	
$\mathbf{A}_{]}$	Appendix A Downscaling Method				
$\mathbf{B}^{\mathbf{i}}$	Bibliography				

List of Figures

List of Abbreviations

au wind stress

 M_e Ekman Transport

 SST_{slw} Low-frequency modulation of SST during upwelling seasonal cycle

TauY meridional wind stress in Chapter 3

 UI_{slw} Low-frequency modulation of upwelling seasonal cycle

AMM Atlantic Meridional Mode

AMO Atlantic Meridional Oscillation

AMO Atlantic Multidecadal Oscillation

ATL-3 Tropical Atlantic

AVISO Satellite altimetry at $1/3^{\circ}$ x $1/3^{\circ}$ resolution provided by Collect Localisation Satellites (CLS, Toulouse, France)

BenCS Benguela Current System

CalCS California Current System

CanCS Canary Current System

EBUS Eastern Boundary Upwelling Systems

ENSO El-Niño Southern Oscillation

EOF Empirical Orthogonal functions

ERAEXP Simulation forced by ERAInterim reanalysis

ERAINT ERAInterim reanalysis

HCS Humbolt/Peru Current System

JRA55 JRA55do v.1.1 reanalysis

JRAEXP Simulation forced by JRA55do v.1.1 reanalysis

MEI Multivariate ENSO Index

NAMM North Atlantic Meridional Mode

NAO North Atlantic Oscillation

NBenCS Northern Benguela Upwelling System - from 14°S-20°S in Chapter 3; from 15°S to 25°S in Chapter 4

NCalCS Northern California Upwelling System

NCanCS - WIP Northern Canary Upwelling System

NCAR National Centers for Environmenta Prediction-National Center for Atmospheric Research

NCDC National Climatic Data Center

NHCS Northern Peru Upwelling System

NH Northern Hemisphere

NOAA SST global SST database from Reynolds et al (2007) in Chapter 2 and 3 and from Smith and Reynolds (2005) in Chapter 4

NPC2-A North Atlantic PC2

NPC2-P North Pacific PC2

NPGO North Pacific Gyre Oscillation

NPMM North Atlantic Meridional Mode

PDO Pacific Decadal Oscillation

PMM Pacific Meridional Mode

QBO Quasi-Biennial Oscillation

Qnet net heat flux - positive downward

RFI Remote Forcing Index

SAAO-A South Atlantic Antarctic Oscillation

SAAO-P South Pacific Antarctic Oscillation

 ${\bf SBenCS}$ Southern Benguela Upwelling System - from 20°S-27° in Chapter3; from 26°S-34°S in Chapter 4

SCalCS Southern California Upwelling System

SCanCS Southern Canary Upwelling System

SHCS Southern Peru Upwelling System

SH Southern Hemisphere

SLP Sea Level Pressure

SPC2-A South Atlantic PC2

SPC2-P South Pacific PC2

SSH Sea Surface Height

SST Sea Surface Temperature

TPDV Tropical Pacific Decadal Variability

UI Monthly Upwelling Index

WSC Wind Stress Curl

WS Meridional wind stress



Chapter 1

Introduction

1.1 Upwelling and Eastern Boundary Upwelling Systems (EBUS)

Upwelling is an oceanographic process in which deep, cold and nutrient-rich waters rise from the deep ocean to the surface. This nutrient-rich upwelled water stimulates the growth and reproduction of primary producers (e.g. phytoplankton) that form the base of the oceanic food web and lead to enhance biological/fish production. Upwelling regions are thus crucial to regulate productivity at global scale and they are important for the global geochemical and biogeochemical cycles. Moreover, upwelling region variability modulates to some extent the basin-scale circulation and and, from a climate point of view, they provide a way by which temperature and salinity of the deeper layers can mix with water masses close to the surface in an ocean that is in general terms stratified. The global ocean presents distinct regions where upwelling is intense, and they can be generally classified in two types: open ocean upwelling and coastal upwelling regions. The three main drivers that work together to cause upwelling are wind, Coriolis effect, and Ekman transport. In the process of upwelling, wind generates net transport of the ocean surface layer (Ekman Transport, M_e) that, due to the Coriolis effect, occurs perpendicular to the direction of the surface wind, at the right (left) in the Northern (Southern) Hemisphere. The M_e follows the equation:

$$\vec{M}_e = \frac{1}{f\rho} \vec{\tau} \times \vec{k} \tag{1.1}$$

where τ is the wind stress, ρ is water density, $\vec{M_e}$ is the Ekman Transport and f is the Coriolis force. If this net movement of water is divergent, then upwelling of deep waters occurs to replace the water removed by M_e . Persistent open ocean upwelling takes place in equatorial regions and in the centre of low-pressure system in subpolar region. In particular, in the equatorial region, the Coriolis force, directed to the right of the trade winds in the Northern Hemisphere and to the left in the Southern Hemisphere, induces a

near-surface Ekman Transport divergence by a net surface water transport at the equator (Figure ??a). On the other hand, coastal upwelling occurs mainly in the subtropics at the eastern side of the basins (Figure ??). In these subtropical regions, the equatorward winds, associated to the semi-permanent subtropical high-pressure systems, are roughly parallel to the meridional orientation of the coastal profiles promoting offshore transport of water directed perpendicular to the wind stress forcing and to the coast. This process generates coastal divergence, and thus, coastal upwelling (Figure ??b). In addition, in these regions, upwelling is also induced by the cross-shore gradients of the surface wind stress, namely the curl of the wind. Indeed, as Figure ??b shows, the drop-off of the wind towards the coast fosters the divergence of the offshore Ekman flows (Bakun and Nelson, 1991), generating the so-called Ekman Pumping $(E_P, Messi\'{e}$ et al. (2009)).

$$E_p = \nabla \times \frac{\tau}{f\rho} \tag{1.2}$$

Positive (negative) wind stress curl in the Northern (Southern) hemisphere favours upwelling.

The major coastal upwelling regions, which are located in in the subtropics at the eastern side of the Atlantic and Pacific Ocean, are commonly known as Eastern Boundary Upwelling Systems. They are the Canary Current System (CanCS, 15°N-44° N, North Atlantic), the Benguela Current System (BenCS,15°S-35°S, South Atlantic), the Humboldt Current System or Peru Current System (HCS, 5° S-40°S, South Pacific) and the California Current System (CalCS, 22°N-45°N, North Pacific) (Figure 1.2), and they are the focus of this thesis. These four regions cover around 1% of the worlds ocean but contain 25% of its biological productivity (Pauly and Christensen, 1995). As mentioned before, the EBUS upwelling is the result of two mechanisms: coastal upwelling and Ekman Pumping. Coastal upwelling is driven by the equatorward wind stress at coast while Ekman pumping by the cyclonic wind stress curl. Since EBUS expand in a large range of latitude, the differences between and within EBUS are latitude-dependent. In particular, in regions close to the Equator, where the equatorward wind are permanent, the upwelling is intense almost year-round (albeit still with seasonal modulation), while in middle latitudes is highly seasonal, with generally higher intensity in boreal (austral) spring and summer in Northern (Southern) Hemisphere domains (Chavez and Messié, 2009). Dynamically, in addition to the upwelling, EBUS regions share common meridional currents as sketched in Figure??. The alongshore winds drive the broad and slow eastern boundary Benguela, California, Iberia/Canary and Humboldt currents, and a poleward undercurrent is generated, over the shelf slope, by the baroclinic modes of the Kelvin coastal trapped waves promoted by the alongshore wind stress (McCreary and Chao, 1985); so that average currents over the water column and within 100 km from the coast are opposite to the surface winds. In term of ocean circulation, the most peculiar among EBUS is the Benguela Upwelling System (Figure ??c). The BenCS is unique in that it is bound between two warm currents: the Angola Current in the north and the Agulhas Current in the south (Hutchings et al., 1998). The Angola Current flows along the narrow shelf of Angola as an extension of the south equatorial counter-current, and forms the northern boundary of the wind-driven upwelling system at the high seasonal Angola-Benguela front (ABF). The Agulhas Current is the western boundary current of the southern Indian Ocean that flows around South Africa and reflects south of Cape Town. The southern boundary of BenCS is defined by the Agulhas retroflection at the southern tip of Africa, where Agulhas Current water penetrates into the southern Benguela. No other EBUS is influenced by another basins' western boundary current. Besides the reported circulation characteristics and their high productivity, many aspects of EBUS dynamics and variability are still not fully understood, leading to unsolved scientific questions (Prospectus for CLIVAR on EBUS 2018, http://www.clivar.org/sites/default/files/Revised-EBUS-Prospectus_July2018.pdf) as discussed in the next section.

1.2 Open Scientific Questions

One of the major concerns related to EBUS is their representation in the numerical models (Cambon et al. (2013a), Richter (2015a), Xu et al. (2014)). Ocean currents, upwelling and the associated biological productivity in the EBUS are largely driven by surface wind stress and, thus the spatial distribution, the depth, and the intensity of EBUS upwelling, in a modelling framework, is strongly affected by the spatial structure of the wind forcing (Small et al. (2015), Fennel and Lass (2007), Fennel et al. (2012), Capet et al. (2004)). The global atmospheric wind products, such as reanalyses, currently used to force ocean and biogeochemical models, usually represent the alongshore wind located too far offshore with respect to observations, leading to patterns of coastal wind curl that favour Ekman pumping rather than coastal upwelling (Colas et al., 2012), and impact alongshore transport (Marchesiello et al., 2003a) and the biogeochemical characteristics of water masses. Even though outlining the improvements of the EBUS dynamics representation is challenged by the relative scarcity of observational data in the ocean, understanding the implications of using different wind forcing in terms of currents, temperature and biogeochemical structure over EBUS is of great importance (EBUS prospectus 2018). These topics, in addition to call for a refinement of the theoretical understanding of the regional circulation in the EBUS induced by the wind, could help to overcome another short-coming of current modelling systems: the well-known warm sea surface temperature (SST) bias in the upwelling regions simulated by ocean and climate models (e.g. Richter (2015a), Xu et al. (2014), Small et al. (2015)). With the twofold objective to increment the present knowledge on EBUS dynamics, and contribute to the understanding of the limitations of the present

ocean modelling tools in simulating it, in Chapter 3 we will discuss the results of two ocean simulations forced by two different atmospheric reanalyses. Another unresolved issue, particular relevant for society, is the EBUS response to global climate changes. Recent studies documented trends (Tim et al. (2015), Wang et al. (2015), Sydeman et al. (2014a)) and decadal scale changes in EBUS. Bakun (1990) hypothesized an increase in upwellingfavourable winds due to intensification of the continental-oceanic pressure gradient under global warming. A more recent hypothesis suggests alternative mechanism, whereby a poleward shift of the oceanic high-pressure system would stimulate latitude-dependent changes in the magnitude and timing of upwelling winds (Rykaczewski et al. (2015a), Wang et al. (2015)). Although the driving mechanism is still being actively debated, previous studies appear to consistently predict that the upwelling favorable in eastern boundary current systems has intensified and that the increasing trend will continue (García-Reyes et al. (2015), Bakun et al. (2010), Garreaud and Falvey (2009)). Even if these studies do not agree whether there is already an ongoing trend in upwelling, nor do they agree on its sign and its causes, part of the long-term variability on EBUS and consequently on their fish resources has been attributed to large-scale, ocean-atmosphere processes (e.g El-Niño Southern Oscillation, Atlantic Meridional Mode). Thus, in order to understand EBUS responses to future climate change, it is necessary to gain a deeper insight into these mechanisms that generate the interannual to decadal variability. We will try to shed some light on them in Chapter 4.

1.3 Thesis objectives

To address the above unsolved questions we will focus on long-term global model outputs. The advantages of treating for the first time these issues in a global framework, instead of most common regional studies (e.g. Xu et al. (2014), Cambon et al. (2013a), Renault et al. (2012)), are the possibility to analyse the coherency of EBUS ocean changes and to address the issue of trends and decadal variability. Moreover, we will present results obtained from a very new atmospheric reanalysis which has been bias corrected to force ocean model, thus, reducing the possible model drifts due to the atmospheric forcing biases typical of atmospheric reanalyses.

In this thesis we raised the following six research questions and addressed them through the chapters.

Chapter2:

- Is the observed variability of wind forcing in EBUS correctly represented in the atmospheric reanalyses?
- Is the observed variability of the ocean dynamical response in EBUS represented in

the eddy-permitting ocean simulations?

Chapter3:

- How does the currents system in EBUS change under different structures of the winds? Are the different EBUS responding in the same way to different wind forcing?
- Are we improving SST biases in an eddy-permitting ocean model using high-resolution atmospheric reanalyses?

Chapter4:

- Which are the drivers of low-frequency variability on EBUS? Are there any trends?
- Is there any shared decadal variability between EBUS? Is that variability driven by climate modes?

Chapter 2 has the main objective to study the variability of the atmospheric reanalyses used to force the ocean model and the analysis of the ocean simulations helped to identify the most relevant questions that have been addressed in the next chapters. Chapter 3 and Chapter 4 present the main results of the thesis and have been prepared for peer-reviewed publication.

Chapter 2

Analysis of the atmospheric and surface oceanic temporal variability in the EBUS

2.1 Introduction

As described in the previous chapter, EBUS are highly productive coastal ocean areas where nutrient rich and cold waters upwell through the action of favourable winds (e.g. equatorward wind stress and cyclonic wind stress curl). These systems provide ecosystem, economic, and recreational services to people living along the coasts and in their immediate inlands. As these systems play a significant role for marine life and hence for the fishing industry, the correct modelling of coastal upwelling patterns, variability and trends is of great importance. Therefore, it is crucial to study and characterize the EBUS observed variability in terms of wind forcing and ocean variables (e.g SST and SSH) and to understand how reanalyses and models reproduce it. Climate model simulations often show significant warm biases in EBUS areas (Cambon et al. (2013a), Richter (2015a), Xu et al. (2014)), preventing reliable representation of the regional variability and motivating detailed studies of the EBUS dynamics in order to understand possible model deficiencies. Here we analyze and validate the EBUS variability coming from long-term ocean hindcast simulations forced by two different atmospheric reanalyses, ERA-Interim (Dee et al., 2011) and JRA55-do-v1.1 (Tsujino et al., 2018). The simulations cover the period 1985-2015 and are performed using a global eddy-permitting configuration (with 1/4° of horizontal resolution) of the NEMO ocean general circulation model. In summary, the present chapter aims: (1) to study and validate the spatial and temporal variability of the wind forcing over EBUS implied by reanalyses, (2) to study and validate the ocean dynamics variability over EBUS forced by the two reanalyses, and (3) to highlight discrepancies between the two simulations, and pose the most relevant questions that will be answered in the next

2.2 Model Configuration and Data

2.2.1 Model description and experiments

The EBUS are investigated in a numerical study based on the state-of-the-art ocean modelling system NEMO (version 3.6), a three dimensional, free-surface, hydrostatic, primitive-equation global ocean general circulation model (Madec, 2015) coupled with the Louvain-la-Neuve Sea Ice Model, LIM2 (Fichefet and Maqueda, 1997) Our configuration employs a global ORCA025 tripolar grid (Madec and Imbard, 1996) with 1/4° horizontal resolution ($\sim 27.75 km$) at the Equator, increasing with latitudes, e.g. $\sim 14 km$ at 60°. The vertical grid has 75 levels, whose spacing increases with a double hyperbolic tangent function of depth from 1m near the surface to $\sim 200m$ at the bottom, with partial steps representing the bottom topography (Bernard et al., 2006). The model bathymetry is based on the combination of ETOPO1 data set (Amante and Eakins, 2009) in the open ocean and GEBCO (IOC, IHO and BODC, 2003) in coastal regions. The horizontal viscosity is bi-Laplacian with a value of $1.8 \times 10^{11} m^4 s^{-1}$ at the Equator, reducing poleward as the cube of the maximum grid cell size. Tracer advection uses a total variance dissipation (TVD) scheme (Zalesak 1979). Laplacian lateral tracer mixing is along isoneutral surfaces with a coefficient of $300m^2s^{-1}$. The vertical mixing of tracers and momentum is parameterized using the turbulent kinetic energy (TKE) scheme. Subgrid-scale vertical mixing processes are represented by a background vertical eddy diffusivity of $1.1 \times 10^{-5} m^2 s^{-1}$ and a globally constant background viscosity of $1.1 \times 10^{-4} m^2 s^{-1}$. The bottom friction is quadratic and a diffusive bottom boundary layer scheme is included. The runoff data are a monthly climatology derived from the global river flow and continental discharge data set (Dai and Trenberth (2002); Dai et al. (2009)) for the major rivers and estimates by Jacobs et al. (1996) for the Antarctic coastal freshwater discharge. The initial conditions from December 1984 are provided by the C-GLORS reanalysis data (Storto et al., 2016) and the simulations cover a period from 1985 to 2015. A pair of modeling experiments that differ only by the atmospheric forcing were conducted to assess the oceanic response in particular to the different winds. The first experiment is forced by ERA-Interim global atmospheric reanalysis (Dee et al., 2011), which has 80km of spatial resolution. The turbulent variables (wind vector at 10 m of height and temperature and specific humidity at 2 m) are given as 3 h mean values, while the radiative fluxes and precipitation are given as daily mean. The second experiment is forced by JRA55-do version1.1 (Tsujino et al., 2018), with 55 Km spatial resolution. JRA55-do-v1.1 is a surface dataset based on JRA-55 Japanese reanalysis (Kobayashi et al. 2015) corrected using different types of observations such as QuikSCAT and ASCAT with the aim to drive ocean-sea ice models. In this case, the turbulent variables, the radiative fluxes and precipitation are all given as 3h mean values. For both experiments the surface boundary conditions are calculated using the CORE bulk formulation proposed by Large and Yeager (2004). Herein after ERAINT and JRA55 identify the atmospheric reanalyses while ERAEXP and JRAEXP the two numerical simulations.

2.2.2 Observations for validation

We use gridded daily wind vector and wind stress fields, estimated over global ocean from QuikSCAT scatterometer data produced and disseminated by Ifremer (Bentamy and Fillon, 2012) to evaluate and characterized the two wind forcing. Wind data from the AS-CAT mission which replaced QuikSCAT since 2008, have been excluded. Indeed, Bentamy et al. (2008) and Bentamy and Fillon (2012) discussed in depth the differences between ASCAT-derived and QuikSCAT-derived wind (hereinafter AS25 and QS25 respectively) showing persistent differences in colocalized wind intensity. Moreover, Desbiolles et al. (2014), comparing them at regional and local scales in the Benguela and Canary upwelling system, argued that QS25 product rather than AS25 shows sharper variability and smaller structures over both regions, and more realistic summer wind stress curl over Benguela region. QS25 spatial resolution is 25km on a regular grid and they are produced from the new QuikSCAT wind retrievals indicated as QuikSCAT V3 (ftp://podaac.jpl.nasa.gov/ OceanWinds/quikscat/preview/L2B12/v3/) with a Wind Vector Cell of 12.5km spatial resolution. The daily wind fields are calculated for the full QuikSCAT V3 period, from October 1999 to November 2009. Data are distributed by IFREMER (ftp://ftp.ifremer. fr.fr/ifremer/cersat/products/gridded/MWF/L3/QuikSCAT/Daily). It is worth mentioning that both atmospheric reanalysis products used in this study assimilate QuikSCAT wind retrievals, while only JRA55 assimilates ASCAT wind retrievals. Futhermore, the version of JRA55 used in this study it also adjusted to QuikSCAT wind, as reported in the new published work by Tsujino et al. (2018). In addition, we use the 25km resolution SST (Reynolds et al., 2007) from National Climatic Data Center (NCDC, hereinafter NOAA SST), over the period 2000-2008 to quantify the simulated SST bias over EBUS. Note that this dataset ingests both day- and night-time bias-corrected SST retrievals from infrared sensors, although night-time measurements are given larger weight than day-time ones. For validation purpose we also used a 23-year time series of satellite altimetry, namely from 1993 to 2015, at $1/3^{\circ}$ x $1/3^{\circ}$ resolution provided by Collect Localisation Satellites (CLS, Toulouse, France; hereinafter AVISO)

2.3 Results

2.3.1 Wind Forcing variability on EBUS

Wind stress

The characterization and the comparison of the two different atmospheric reanalyses used to force the ocean simulations in terms of meridional wind stress (WS) and wind stress curl (WSC) is the focus of this section. If not otherwise specified, all the results presented in this section are computed over the 2000-2008 period, and the areas considered are BenCS (15°S - 34°S), Moroccan and Gulf of Cadiz sectors for CanCS (24°N-34°N), CalCS (27°N-44°N) and HCS (5 °S - 35 °S). In order to explore the temporal and spatial variability of the wind forcing over EBUS we first examine the characteristic of the wind stress and wind stress curl climatology. Figure ?? and Figure ?? show the mean WS and WSC derived from the considered atmospheric products over the four upwelling regions. The dominant spatial patterns, as described in Chapter 1, are characterized by cyclonic curl near coastal boundaries and anticyclonic curl offshore, in association with equatorward alongshore (upwelling-favorable) wind stress. Over the Atlantic areas (Figure ??a and c top panels), QuikSCAT wind stress maxima are usually associated with the presence of a cape: Cape Frio (16°S), Lüderitz (27°S) and Cape of Good Hope (34°S) in the BenCS, and Cape Sim (31°N), Cape Juby (34°N) and Cape Blanc (22°N) in the Canarian region. On the Pacific side (Figure ??b and d, top panels), California maxima are situated at Cape Mendocino, at 40°N, and at 43°N, and Peru maxima at 31°S and 14°S. The annual mean maximum wind stress exceeds $0.15 N/m^2$ in the California system. The wind from both atmospheric reanalyses reproduces the overall patterns, but the WS fields present an offshore easterly wind underestimation in the northern (southern) part of the Northern Hemisphere (Southern Hemisphere) domains and an evident coastal bias (100km) when compared to QuickSCAT data. Discrepancies among the products are also evident in WSC patterns (Figure ??): ERAINT reanalysis presents usually wider (except for Peru system) and stronger WSC with respect to JRA55 that, even with lower maxima, better resembles QuiKSCAT WSC. Differences in WSC, especially the overestimation using the ERAINT reanalysis, are due either to strong wind drop off near the coast or offshore position of wind maxima linked to atmospheric resolution. Wind drop off representation and its role in driving the ocean circulation are treated in details, for upwelling season, in Chapter 3. Both reanalyses, even though with significant differences in the coastal zone, show a good representation of the wind mean state. Since EBUS are temporally and spatially heterogeneous environments (Wooster, 1963) and they can be divided in subregions in light of the temporal variability of the WS (Chavez and Messié, 2009), we now explore the wind forcing temporal and spatial variability in the different products.

Figure ?? shows an Hovmoller diagram of QUIKSCAT meridional wind stress (2000-2008) averaged over a region of 100km (4 grid points) from the coast. Positive (negative) values in SH (NH) are upwelling favorable winds. The Benguela region, as the mean-state pattern suggests (Figure ??), could be divided in three sub-regions: Northern Benguela (14°S-22°S) with year-round upwelling favorable wind and wind maxima localized at Cape Frio during the austral summer and fall, Central Benguela (22°S-30°S) dominated by the Lüderitz upwelling cell at 27°S with maxima during the austral summer, and Southern Benguela (30°S-34°S) associated with seasonal upwelling during the austral summer, especially at Cape of Good Hope (34°S). Remaining on the Atlantic sector, the Canary coastline and climatological Hovmoller suggest two different sectors: the Moroccan sector (20°N-31°N) that experiences year-round upwelling with maximum in boreal summer/spring, and the Senegal sector (15°N-20°N) with boreal winter-spring upwelling and different coastline orientation. On the Pacific side, the California region can be divided by two main capes: Cape Mendocino (40°N) and Cape Conception (34°N). Northern California (40°N-45°N) exhibits seasonal upwelling in boreal summer with wind maxima of $0.15 N/m^2$, Central California (40°N-34°N) is characterized by upwelling-favorable wind all year-round with a maxima during the boreal summer, whereas Baja California (34°N-27°N) presents a weaker upwelling throughout the entire year. Four main regimes, based on latitude, can be identified in the Peru area: a central Peru upwelling regime with maximum upwelling in the austral winter between 5°S and 16°S, a southern Peru-northern Chile transitional regime with weaker upwelling throughout the year between 16°S and 26°S, and two central Chile regimes with maxima upwelling in the austral spring (26°S-32°S) and summer (32°S-37°S), respectively. Note that all these regimes are upwelling-favorable throughout the year, except over CalCS at 35°S-40°S in late fall-early winter. Qualitatively similar regimes are present in the ERAINT and JRA55 (not shown). Therefore, to better understand the WS-WSC spatial and temporal variability and their representation in reanalysis products, a Fourier transform analysis has been performed on WS and on WSC (Figures ??-??-??), following Chavez and Messié (2009). The Fourier Transform is performed on the daily WS or WSC times series after removing their respective linear trends. Then, for each selected timescale (annual, semi-annual, longer than semi-annual) an inverse Fourier transform is performed by keeping the Fourier coefficients corresponding to that time scale and reconstructing the corresponding time series. The ratio of the variance of the resulting time series to the variance of the full-time series, previously calculated, gives the percentage of variance explained by each time scale. Looking at the QuikSCAT solution (Figure ??a, first column), the Benguela system is dominated by seasonal variability south of 24°S and by semi-seasonal (6 months) and higher frequency north of 24°S. The Canary system (Figure ??b, first column) shows seasonal variability south of 15°N and at Cape Blanc (22°N), high frequency north of it and roughly equal levels of semi-annual and higher frequencies in the

Moroccan sector. The Pacific regions, as Figure ??a,b first column reports, have a much higher proportion of their variance at seasonal scales except over some particular areas such as between 31°S-29°S in Peru and over Baja California, between 29°N-34°N, where they have variability on higher frequencies. Reanalyses properly represent the offshore amplitude and the location of total variance. On the other hand, because of weaker WS at coast, ERAINT always shows a smaller variance near the coast (Figure ??-?? second column, total variance row). Regarding the variance decomposition, there are no particular differences among all the products except south of Cape Mendocino (in California at 40°N, Figure ??b) and on the Moroccan sector (Figure ??b) where atmospheric reanalyses present seasonal variability. The only remarkable difference between the two products is in the Benguela system north of 15°S, where JRA55 has higher variability (Figure ??b, < semi-annual row).

Wind stress curl

Moving on to WSC, as shown by the Hovmoller diagram of the WSC anomaly in Figure ??, in all the EBUS it has a distinct seasonal cycle that is relatively homogeneous in latitude. It is worth noting that the plotted variable is the WSC anomaly, thus negative (positive) anomaly on SH (NH) indicates strong WSC with respect to the long-term mean over the QuickSCAT period. In general, the eastern upwelling systems show strong WSC during wind maxima and therefore during upwelling season. Comparing QuikSCAT variability with the reanalyses variability (Figures?? and??), besides some missed semiannual scale at Cape Frio (Benguela, 17°S, Figure ??a, second row) and the more defined annual cycle along Peru coast (Figure ??a, first row), the atmospheric reanalyses suffer by total variance and offshore high frequencies variability deficits. In particular, the former deficit is evident along Benguela System nearby Lüderitz (Figure??a, total variance row), along Senegal sector (Figure ??b, total variance row) and along California coast (Figure ??b, total variance row), while the latter is particularly clear in the Peru system between 17°S-27°S (Figure ??a, third row). It is worth noting that the California area exhibits the most significant discrepancies among all the reanalyses (Figure ??b): the coastal zone between 36??N-45??N is dominated by annual cycle in the ERAINT product, while by higher frequency in JRA55 and data estimations. Focusing on the coastal total variance deficit, the time series of ERAINT WSC computed at 44°N (red line of Figure 8a) presents higher standard deviation than JRA55 and QuikSCAT with values of $4.2e - 7Nm^{-6}$ with respect to $2.7e - 7Nm^{-6}$ and $2.8e - 7Nm^{-6}$ for JRA55 and observed data, respectively. Nevertheless, correlations with observed data are high for both reanalyses, 0.68 for ERAINT and 0.78 for JRA55. Controversially, the WSC times series for the Canary system at 20°N (Figure ??b) is characterized by much larger QuikSCAT standard deviation (value of $1.2e-7Nm^{-6}$ for QuikSCAT, $8.8e-8Nm^{-6}$ for ERAINT and $8.9e-8Nm^{-6}$ for JRA55) and reanalyses present quite low correlations, 0.38 ERAINT and 0.41 JRA55. In summary, despite some localized differences near the coast, both reanalyses, and especially JRA55, represent accurately the WS variance, amplitude and seasonality, while they exhibit some discrepancies in the WSC amplitude and variability. In particular, they do not properly capture the wind drop-off, too strong in ERAINT and too weak in JRA55 compared to QuikSCAT.

2.3.2 Ocean dynamical response

In this section we start to explore the temporal and spatial variability of the ocean forced by the two reanalyses in terms of the response of surface oceanic variables. In this chapter, in contrast to Chapter 3, I will focus just on SSH and SST dynamical response. This is due to the fact that the main intent of this analysis is to validate modelled fields with available observational-based global dataset instead of understanding process. In fact, we validate the surface oceanic response using AVISO for SSH and NOAA SST for SST.

Sea Surface Height

To understand the predominant variability of the surface ocean in each EBUS we analyze SSH. Using the same technique applied to the WS and WSC, a 23-year time series of AVISO data and of simulated SSH were analyzed for each of the four EBUS regions, and the percentage of the variance explained by interannual, seasonal, and intra-seasonal scales calculated (Figures ??-??-??). It is worth mentioning that this analysis differs from the previous presented in Figures ??-??-??: here we considered bigger areas in order to identify large-scale features; interannual (>1 year) and intraseasonal (<1 year) variability are considered and seasonal variability corresponds to annual cycle (1-year frequency). The same analysis is presented in Chavez and Messié (2009) for AVISO altimetry data for a shorter period (1993-2006). In our case, the main purpose is to use it to validate the simulated SSH. In general, looking at the results obtained from AVISO altimetry data, we find the same results reported by Chavez and Messié (2009). The Benguela system is dominated by intra-seasonal variability (Figure??, first column), presumably due to eddy activity and the high variability driven by the interaction of the warm Agulhas Current (and its retroflection) with the upwelling areas through Cape de Good Hope (34°S) is clearly outlined in the total variance (Figure ??, bottom row). Nevertheless the total variance does not precisely match the percentage explained by intra-seasonal variance suggesting that part, but not all of the eddy activity is a result of this interaction. Remaining on SH (Figure ??, first column), Peru has a much higher proportion of its variance at interannual scales, especially along the coast where El-Niño dynamics dominates (5°S-15°S), while along Chilean coast (28°S-32°S) the systems is mostly intra-seasonal driven suggesting intense eddy activity,

as suggested in Combes et al. (2015). In the NH, the Canary system variability is highly seasonal, except in the 10°N-5°N latitude range, where the intra-seasonal easterly wind migration prevails (Figure ??, first column), and the California seems to have roughly equal levels of interannual, seasonal and intra-seasonal variability (Figure ??, first column). The overall features depicted by AVISO are well represented in the JRAEXP and ERAEXP simulations. Both simulations tend to underestimate intra-seasonal variability, likely due to the limitation of NEMO configuration to resolve the mesoscale which can play an important role in these areas (see Cessi and Wolfe (2009), Combes et al. (2013) and Combes et al. (2015)). This is particularly evident over the Benguela and Peru regions (Figures ?? and ??, intraseasonal row): the underestimation of intraseasonal variability is compensated by an excess of variance at interannual scale for the ERAINT-forced ocean and at seasonal scale for the JRA55-forced ocean simulations.

Sea Surface Temperature

Another important variable to validate is the SST. The issue of coastal SST in EBUS simulated by climate and ocean models has being vigorously investigated, since SST bias is pervasive across many models (Tim et al., 2015). The reason is still not completely clear, as it has been recently reviewed by Richter (2015b). Both atmospheric and oceanic processes may be involved: stratiform clouds in the boundary layer, too weak winds, and remote oceanic influence from the tropics may all play an important role in the resulting SST warm bias (Richter, 2015b). As mean state of SST displays for each EBUS (Figures?? ?????, top panels), our simulations, especially along the coast, suffer as well by SST bias if compared to NOAA SST (Reynolds et al., 2007) which is used as our reference for the entire simulated period (1985-2015). Generally, the SST in the simulation driven by JRA55 results colder than ERAEXP SST but warmer than NOAA data set (Figures ??b-??b-??b-??b, first row), namely the use of JRA55 mitigates the warm bias of ERAEXP Along Chile coast, Lüderitz and Cape Sim (at 31°N) in Canary System, and induces SST colder than observed in some areas (Fig. ??c-??c-??c, first row). Nevertheless, the areas interested by cool water (e.g area of upwelling) have the same spatial distribution in the reanalysis and in the data. Minima are localized over the Lüderitz cell (Benguela, 27°S), NW Africa (25°N-30°N), along Oregon and California coast and along Chile coast (Peru System, 27°S-30°S). The SST bias and its causes are treated in more details and during each EBUS relevant upwelling season in Chapter 3. Regarding the SST variability, in particular its annual cycle, Figure?? shows the Hovmoller diagram for each area of NOAA SST averaged over a region of 100km (4 grid points) from the coast (JRAEXP and ERAEXP Hovmoller report similar variability to the observed one, thus, they are not shown). As expected, the SST is warmer equatorward and has a pronounced seasonal cycle, with maximum in boreal (austral) summer in NH (SH). Around 15°S-17°S in the Benguela region, the AngolaBenguela Front (ABF) is represented with its seasonal variation (e.g. northernmost in boreal summer) and the intrusion of equatorial water during austral winter (DJF) is a clear feature over the Peru system. It is worth mentioning that the seasonality of upwellingfavourable winds does not correspond to a clear signature on SST (see Figure?? and Figure ??), indicating that SST itself cannot be taken as an index of upwelling seasonality since it is influenced also by other factors (e.g. heat fluxes and advection, see Chen et al. (2012) and McCabe et al. (2015)). In terms of total variance, as Figures?? and?? depict, data and simulations behave in a very similar way: they show high variability over Angola Benguela Front, north Peru (e.g. where El Nino has major impacts, Tarazona and Arntz (2001)), Baja California and Senegal sector where upwelling is seasonal (see Hovmoller of wind stress Figure ??). Not surprisingly, in the areas where upwelling is permanent we have the lowest total variance, indeed these areas experience cold temperature all year around. As expected from the SST dynamics, more than 60% is explained by the annual cycle (Figures?? and??, seasonal scale row), especially offshore. On the other hand, along the coast part of the variance is explained by intra-seasonal scale (e.g. upwelling events and eddy activity) and on Pacific coast also by interannual scale (coherent with SSH analysis). Regarding the validation of our simulations, no particular differences are evident among them except at intra-seasonal time scale where simulations reveal higher variability than NOAA SST analyses. The only remarkable difference between the two simulations is in the Benguela system north of 15°S, where the JRA55 based simulation has higher total variance than the ERAINT one (Figure ??a, total variance row). Even though the SST variability is definitively well captured, the trends over the simulated 30 years result different between the NOAA SST and simulations over the Atlantic domains (Figure?? and??, second row). Benguela simulated trends result positive around Cape Frio and negative elsewhere, while NOAA SST experience positive trends almost everywhere. Over NW Africa, as reported by Gómez-Letona et al. (2017), trends computed from SST data show significant overall warming tendency especially on the southern part while our simulations suggest intense cooling over Moroccan Sector and warming elsewhere. Pacific modeled results, especially JRAEXP, and NOAA data appear to be in line with observation, at least in the sign of the tendency (Figure ?? and ??, second row). ERAEXP trends are in general stronger than the other two products. These discrepancies pointed out another important issue in climate and ocean study, in particular over EBUS: the trends and their dependence on climate variability. We will treat this argument in more details in Chapter 4.

2.4 Discussion and Conclusion

In this chapter, we investigated the variability of EBUS through an analysis of atmospheric reanalyses, ocean numerical simulations and observational data. We focused in

particular on the analysis of the wind forcing and SSH, SST responses. These EBUS characteristics have been investigated in two numerical simulations performed using a NEMO global ocean configuration at 1/4° horizontal resolution, sharing the initial condition but forced by ERA-Interim and JRA55 reanalysis, respectively. We found that the variability of the wind forcing is mostly seasonal and the differences in wind forcing within EBUS are latitude-dependent. Low latitude experience mostly year-round upwelling favourable wind (even though still with seasonal modulation), while at higher latitudes upwelling favourable winds typically occur in boreal (austral) spring and summer in NH (SH) systems. The two atmospheric forcing depict the observed variability, presenting some difficulties mainly in the coastal regions. In particular, maxima of the wind appear always too far from the coast and the wind stress curl too strong. These discrepancies, in light of the importance of the wind over these areas (e.g Marchesiello et al. (2003a), Capet et al. (2004), Small et al. (2015)), arise the first important unsolved question: how are the upwelling systems affected by coastal wind forcing biases (Chapter 3)? Furthermore, they highlight the need to high resolution wind forcing at coast. Thus, low computational demanding methods, such as statistical downscaling (Appendix A, Goubanova et al. (2011), Cambon et al. (2013a)) are of great importance to enhance resolution of atmospheric reanalyses at coast and to potentially better solve EBUS ocean dynamics (Chapter 4). By studying the ocean variability, our results show that also SST and SSH are well represented in the simulations. Nevertheless, the principal feature that emerges from the variability analysis over the ocean is that the character of the four EBUS is to a first order dependent on basin-scale features: Pacific, especially Peru system, is dominated by interannual variability (e.g. ENSO dynamics), Benguela system by eddy-induced variability (intraseasonal variability) due to lateral remote advection from Indian Ocean, while Canary is mainly dominate by seasonal variability, likely due to an important seasonal cycle in heat forcing and SST (Arístegui et al. (2009), Pelegrí et al. (2005)). On the other hand, in all EBUS, SST variability results highly seasonal offshore and intraseasonal at coast, influenced by upwelling events. Moreover, analysis on SST annual cycle reveals a missing matching between the coolest temperature and the upwelling favourable winds, indicating SST as a not adequate index for upwelling, as several authors already pointed out. Chen et al. (2012), for instance, defined an index derived from the SST and mentioned that it represents well the upwelling intensity in terms of the spatial variation but not the temporal variations. In general, SSTs are not only affected by upwelling but also by a complex interaction between horizontal ocean advection, ocean-atmosphere heat fluxes, and vertical mixing (McCabe et al., 2015). Moreover, SST linear trends among the products are significantly different. SST simulated trends resemble each other while they present large differences with our SST reference (NOAA SST). In literature, recent studies (Sydeman et al. (2014a), Narayan et al. (2010)) do not agree whether there is already an ongoing trend in upwelling, nor do they agree on its sign. The result of the trend analysis depends on the type of data set used, the temporal coverage and variable used as indicator for upwelling. Therefore, more sophisticated index, such as release of passive tracer at subsurface, and longer simulations shall be considered for these areas in order to study trends and low-frequency variability (Chapter 4). In summary, answering to the goals presented in the introduction, the variability analysis of EBUS using atmospheric reanalyses, ocean simulations and data suggest:

- 1. variability of forcing is mostly seasonal and it is well represented by reanalysis product, even though they exhibit coastal biases;
- 2. variability of SST is mostly seasonal in all the EBUS, while SSH highlighted different predominant time scales in each EBUS: variability is seasonal over CanCS, intraseasonal over BenCS, interannual in HCS and mixed in CalCS. These variabilities are caught by ERAEXP and JRAEXP but SST trends are not well reproduced. In fact an overall warming in Northern Benguela and along Canary coast are absent in our solutions;
- 3. the need to study the role of coastal wind on ocean response (Chapter 3), and the need to quantify trends and low-frequency variability using a proper index of upwelling in an ocean model forced by enhanced resolved wind forcing (Chapter 4). These open issues are discussed in details in Chapter 3 and 4, respectively.

Chapter 3

EBUS response to different atmospheric forcing in a global eddy-permitting ocean model

3.1 Introduction

Upwelling systems, especially along eastern boundaries, are characterized by a combination of dynamical processes which are not yet completely understood, and certainly not well enough represented in ocean and coupled models (e.g. Richter (2015b), Xu et al. (2014), Small et al. (2015)). The four main EBUS are the most important productive marine regions that climate models, as well as ocean models, find the hardest to properly simulate: warm sea surface temperature biases, especially during upwelling season, are common problems whose origins remain highly controversial. These biases strongly limit the predictability of future evolution of these regions and, moreover, they have significant remote effects on surface and subsurface temperature and salinity, and on precipitation, influencing atmospheric heating and circulation (Collins et al., 2006) with feedbacks to the large-scale climate system (Large and Danabasoglu (2006); Curchitser et al. (2011), Small et al. (2015)). Several factors may contribute to the erroneous SST representation in the climate models: (1) underestimated stratocumulus decks in the atmospheric models, leading to excessive shortwave radiation at the ocean surface (Hu et al. (2008), Huang et al. (2007a)), (2) remote forcing, especially along Benguela Upwelling System (Xu et al. (2014), Junker et al. (2015)) (3) mesoscale eddies and their contribution to offshore transport (Toniazzo et al. (2010), Zheng et al. (2010)), and (4) alongshore winds, wind stress curl and turbulent fluxes, partially due to resolution issues (Richter (2015a), Colas et al. (2012)). Ocean-only studies could highlight the primary importance of the mesoscale eddies and the wind pattern over EBUS. In this work we will focus in particular on the relevance of different wind patterns. In the eastern upwelling areas persistent equatorward wind stress

(TauY) plays a dominant role in determining coastal upwelling and equatorward currents (Bakun, 1990), whereas permanent cyclonic wind stress curl (WSC) controls Ekman pumping and, by consequence, modulates vertical advection (Wooster (1963), Bakun and Nelson (1991); Albert et al. (2010)). Thus, the alongshore equatorward wind stress and the crossshore gradient of winds toward the coast with their respective Ekman mechanisms, are the main drivers of the upwelling areas Fennel and Lass (2007), shaping the full three dimensional ocean circulation (Marchesiello et al. (2003a), Gill (2016)), as well as partially determining the sea surface temperature structure (e.g. cooling at coast). Because of this predominant wind-driven dynamics, understanding how EBUS coastal currents change under different atmospheric forcing is of primary importance, in order to shed some light on the wind contribution to SST biases. The EBUS sensitivity on the precise structure of the wind stress and wind stress curl near the coast has already been treated theoretically in linear models by McCreary and Chao (1985), focusing on the California Current System, and by Fennel et al. (2012) in the Benguela Upwelling System. Both studies demonstrated that a downwind coastal jet forms in the upper ocean, with an underlying deep poleward undercurrent (PUC), when the maximum of the alongshore atmospheric jet has an inshore location. In contrast, for atmospheric jets sufficiently detached from the coast, the WSC structure is broad in the zonal direction promoting weak equatorward coastal jet at the boundary and the shoaling of the undercurrent as counterflow (McCreary and Chao (1985), Fennel et al. (2012), Fennel and Lass (2007), Albert et al. (2010)). Beside the consequences on meridional velocities, the existence of WSC and TauY inshore location significantly shape the vertical velocity over the continental shelf: Ekman Pumping enhances if the maximum of the wind stress is far from the coast, while coastal upwelling dominates when strong TauY is present at coast.

In a numerical modelling framework, both the ocean model resolution and the representation of the atmospheric forcing may play a crucial role for ocean and climate oriented studies (Desbiolles et al. (2014), (Capet et al., 2004), Small et al. (2015)). In this matter, Small et al. (2015) in their recent work have reported significant improvements in upwelling dynamics and sea surface temperature representation increasing atmospheric resolution rather than the ocean one. In fact, simulations forced by low resolution atmospheric forcing, which are dominated by stronger WSC and weak coastal winds, usually present the shoaling of the poleward and warm undercurrent and weak coastal upwelling. On the other hand, the increase of the atmospheric forcing resolution results in a strengthening of coastal winds and a narrowing of the WSC, which promote strong coastal upwelling, enhanced coastal jet and so, cold advection from the deep ocean and from the pole. Therefore, a more realistic wind pattern to force ocean model could improve the understanding of coastal currents (Marchesiello et al., 2003a) and it could significantly contribute to reduce the SST biases over the eastern boundary systems (Small et al. (2015), Capet et al. (2004))

due to a reversal of sign of the meridional flow, from poleward (warm advection) to weak equatorward (cold advection), due to the concurrent increase of coastal upwelling (Small et al. (2015), Renault et al. (2012), Marchesiello and Estrade (2010)), and due to the increase of turbulent fluxes. Furthermore, the different simulated current and temperature structures induced by different wind forcing may have impacts on the whole ecosystem and production, strongly influencing the composition and the biogeochemical characteristic of the upwelled water (Blamey et al. (2015), Hutchings et al. (1998)). The composition of this water is, indeed, largely affected by the strength, the direction and, especially, the depth of the coastal currents (Junker et al., 2015). Thus, to quantify and to report the improvements and the implications of using different atmospheric forcing is of great importance also for ecosystem and ecological study that are oriented to understand the evolution of these areas in a changing climate (EBUS prospectus). Motivated by these assumptions, in a climatological oriented framework the main objectives of this study are (1) to validate, study and characterize wind forcing from new-released atmospheric reanalysis over EBUS, (2) to understand the sensitivity of currents and temperature structure to changes in the atmospheric forcing in all EBUS and, (3) to quantify the equatorward (e.g. coastal jet) and poleward (e.g undercurrent) meridional transport changes induced by the forcing. For these purposes, we use the NEMO global ocean model with 1/4° resolution forced by two atmospheric reanalysis products: Era-Interim (Dee et al., 2011) and a newly available bias-corrected version of the JMA JRA55 reanalysis (JRA55-do v.1.1, Tsujino et al. (2018)). The advantage of treating for the first time this issue in a global framework is the possibility to analyse the coherency of ocean changes to atmospheric forcing in order to identify a common response among the EBUS. The paper has the following structure. The data and methods are described in Section 2 and the results in the following one. Firstly, the reliability of wind forcing in comparison to QuikSCAT satellite wind stress is shown (Section 3.3.1). Secondly, the response of the EBUS ocean currents (Sect. 3.3.2) and sea surface temperatures (Sect. 3.3.3) to the different forcing is presented. Finally, these results are discussed in Section 3.4 together with the most important conclusions.

3.2 Model Configuration and Data

The model configuration, the experiments and the data are the same of Chapter 2.

3.3 Results

If not otherwise specified, all the results presented in this section are computed during the upwelling season (from October to January in the SH, and from May to August in the NH) over the 2000-2008, and the areas considered are Northern Benguela (15°S - 29°S

), Gulf of Cadiz sector for CanCS (24°N-34°N), Northern and Central California (35°N-44°N) and Central Chile (35°S-25°S). We chose 2000-2008 period for validation reason (e.g QuikSCAT available period). For thesis coherency the four domains will be identify as BenCS, CanCS, CalCS and HCS through the text and the figures even if the areas investigated are slightly different (e.g smaller) than in Chapter 2.

3.3.1 Wind Forcing analysis in the EBUS

One of the aim of this study is to assess the quality of the wind fields in the two atmospheric reanalysis products, thus, we validate them against the higher resolution QuikSCAT estimates. The differences between ERAINT and JRA55 winds are discussed, instead, in more details in the next section in the context of their influence on ocean response. Figures ??,?? and ?? show the seasonal upwelling mean of TauY and WSC for the study period. In this work, the meridional wind is used in the wind stress (TauY) computation being the upwelling favourable component over the majority of the domains, due to the north-south orientation of the coastline, especially near the capes, where the upwelling activity is maximum (García-Reyes and Largier (2012)).

In all the products the dominant spatial patterns are characterized by cyclonic curl near continental boundaries and anticyclonic curl offshore, in association with equatorward (upwelling favourable) wind stress (Figures ??,??). In the Atlantic, the wind maxima are usually associated with the coastline geometry that includes a cape: Cape Frio (16°S), Ludernitz (27°S) and Cape of Good Hope (34°S) in the BenCS, Cape Sim (31°N) and Cape Juby (28°N) in the CanCS. In the Pacific, California maxima are situated at Cape Mendocino (40°N) and at 43°N, whereas HCS maxima at 31°S. Based on Figures ??,?? and ??, we can argue that both reanalyses reproduce the overall observed patterns, but TauY fields present an evident negative coastal bias within $\sim 100km$ from the coast, especially in ERAINT. To further investigate this bias, Figures??-??a shows the meridional wind stress (TauY) along the coast (e.g. at the closest ocean grid point to the coast) as a function of latitude. ERAINT underestimates QuikSCAT TauY at coast, especially in wind maximum regions and along the HCS coast, while JRA55 winds resemble much better the observed latitudinal variation except in the California region at $\sim 43^{\circ}N$, where winds are underestimated. Nevertheless, the major discrepancies are evident in the cross-shore profiles of the equatorward wind stress (Figures?? and??, top panels). QuikSCAT profiles show strong coastal wind with inshore location of the maxima resulting in narrow and not sharp drop-off on BenCS, CanCS and CalCS while it depicts strong and almost constant winds offshore HCS. JRA55 winds, which are biased corrected using QuickSCAT, mirror the coastal winds amplitude and location of maxima, while ERAINT profiles underestimate nearshore wind and presents maxima located offshore. The wind drop-off discrepancies among products at selected latitude (Figures ?? and ??) are representative of WSC patterns alongshore: ERAINT presents strong WSC on all the domains whereas observation-based products and JRA55 show narrower and weaker WSC in BenCS, CanCS and CalCS and almost absent WSC along the coast of HCS (Figures ?? and ??). In spite of the low accuracy of scatterometers data near the coast (a few tens of kilometers off the coast) we can argue that JRA55 winds, as biased corrected winds, represent more accurately the coastal wind patterns, even with some underestimation on BenCS and overestimation in North California (43°N).

3.3.2 Coastal Currents in the EBUS

To investigate the mechanisms by which the different TauY and WSC drive upwelling velocity and meridional currents and transport in the global model we first study the differences in TauY and WSC between the two products (JRA55-ERAINT). As a Figure ?? shows, along HCS and CalCS coasts JRA55 has stronger TauY and weaker WSC at coast, highlighted by positive (negative) differences in the SH (NH). Patterns of differences are patchy for BenCS and CanCS systems, nevertheless near the capes, where the upwelling activity is maxima (García-Reyes and Largier, 2012), JRA55 TauY results stronger and its gradient weaker. The differences in term of Tauy and WSC in the areas interested by wind maxima (usually the capes, see Figures ??-??) reach values of 0.45 (-0.45) dyn/cm^2 and 5E-7 (-5E-7) N/m^3 in SH (NH) EBUS, roughly the 20% of the absolute values. According to the mechanism suggested in the introduction, differences in TauY are reflected in differences in currents (compare Figure ?? top panel with Figure ?? bottom panel): stronger TauY at coast in the JRAEXP simulation intensifies downwind currents or weakens the poleward flow in the case of Angola current (poleward current in North Benguela, see Figure ??) up to $9cms^{-1}$. Furthermore, current maxima move toward the coast giving nearshore positive (negative) differences at coast and negative (positive) differences offshore in SH (NH) systems. This signal is less evident along Canary coast, expect for the area around Cape Blac (31 °N), likely because of the complexity of the topography in this area (Arístegui et al., 2009). In terms of vertical velocities TauY affects coastal upwelling, in fact we find localized and intensified coastal upwelling in JRAEXP solutions in a coastal strip of 10-30km (see Figure ??, top panel), characteristic scale of this process (Marchesiello and Estrade, 2010). Differently from TauY, discrepancies in WSC should imply differences in Ekman pumping-induced upwelling velocity and differences in undercurrent strength and depth. The former mechanism is confirmed in Figure ?? (bottom panel): since Ekman Pumping dominates offshore at larger scale than coastal upwelling (usually the scale of the wind drop-off, Marchesiello et al. (2003a)), ERAEXP vertical velocities (Figure ??, middle panel), that are driven by stronger and wider WSC, clearly result ex-

panded offshore. Thus, as shows in Figure ?? (bottom panel), positive differences (due to stronger nearshore velocities in JRAEXP experiment) are surrounded in all domains by offshore negative differences (due to stronger Ekman Pumping-induced vertical velocity in ERAEXP). These discrepancies are further evident analysing the cross-shore profiles of vertical velocity together with meridional wind stress at WSC/TauY differences maxima, namely at 27°S in BenCS, at 31°N in CanCS, at 39°N in CalCS and at 31°S in HCS (Figures ?? and ??). ERAINT wind profiles (red line) exhibit wind stress drop-off from $0.12 N/m^2$ to $0.08\ N/m^2,\, 0.06\ N/m^2$ and $0.02\ N/m^2$ in BenCS, CalCS and HCS respectively and from $0.10 \ N/m^2$ to $0.03 \ N/m^2$ in CanCS. The corresponding JRA55 profiles (yellow line) are smoother, especially in the HCS, more confined at coast with wind values greater than 0.02- $0.03 \ N/m^2$ with respect to ERAINT. The offshore upwelling velocities, considered as an index of Ekman Pumping, reproduced by ERAEXP are wider and stronger in accordance with wind drop-off length, whereas enhanced velocities occur at the coastal upwelling scale (about 30km) in JRAEXP forced solution associated to the stronger TauY at coast. Given the vertical velocity changes, differences in WSC also imply differences in undercurrent: JRAEXP case presents, in Figure ??, deep poleward undercurrent, with an average velocity of |5cm/s|, while the corresponding vertical structure from ERAEXP shows stronger and shallower undercurrent particularly fast over the continental slope in CalCS and HCS. Moreover, as mentioned when we discussed surface currents variations, JRAEXP solutions are characterized by enhanced coastal jet downwind (equatorward) with an average speed greater than |12cm/s| in the shallow boundary layer whereas ERAEXP by weaker coastal jet. Having described the link between wind forcing and coastal currents, we now examine and quantify the changes in meridional transport. To address this task we compute a Hovmoller diagram of the climatological meridional transport (averaged along the latitude and integrated from coast to 150km offshore, Figures??-??-??) as a function of depth, and then we quantify the upwelling seasonal equatorward and poleward transport (averaged along the latitude and integrated over the first 300m of water column and from coast to 150km offshore, Table 3.1). In this analysis we consider two distinct areas in the Benguela region due to the different ocean dynamics dominated by Angola current (NBenCS, 14°S-20°S) in the northern part of the region and by Benguela current (SBenCS, 20°S-27°S) in the southern one. Because of the meridional circulation characteristic along EBUS coast (e.g. coastal jet at surface and undercurrent below), we will consider equatorward transport as coastal jet transport (CCT), while poleward transport as undercurrent transport (UCT), expect on NBenCS in which the poleward transport is due to Angola current. Although both experiments show the same meridional transport variability through the year, the intensity and the depth of the boundary-currents transport differ completely (Figures??-?? and ??). Principal discrepancies are evident over the first 70m along NBenCS, SBenCS, CalCS and HCS systems, and over the whole water column for CanCS: JRAEXP solution

	JRA	EXP	ERAEXP			
	CCT	UCT	CCT	UCT		
NBenCS	0.05 Sv	-1.69 Sv	0.02 Sv	-2.14 Sv		
SBenCS	0.13 Sv	-1.3 Sv	0.08 Sv	-1.4 Sv		
CanCS	-1.2 Sv	0.49 Sv	-0.76 Sv	0.70 Sv		
CalCS	-0.88 Sv	0.77 Sv	-0.46 Sv	1.30 Sv		
HCS	0.5 Sv	-0.8 Sv	0.3 Sv	-1.88 Sv		

Table 3.1: Table 1 Equatorward (CCT) and poleward (UCT) transport in Sv ($10^6m^3/s$) for JRAEXP and ERAEXP experiments for all the EBUS, averaged along the latitude and integrated in 150km offshore. Period: upwelling season, (2000-2008).

is characterized by stronger and deeper transport in the direction of the wind (equatorward, negative in NH and positive in SH hemisphere) with peak during upwelling season (red squares), while ERAEXP shows equatorward transport just at surface. In accordance with these inequalities, ERAEXP undercurrent transport (positive in NH and negative in SH) results shallower than JRAEXP, and, especially in HCS, extremely stronger. Furthermore, it worth mentioning the peculiar seasonal variability of CanCS and CalCS meridional transports (Figure ??): they experience months (e.g from January to June in CanCS and from March to June in CalCS) characterized only by coastal jet (negative) transport.

Quantitatively, as Table 3.1 shows, in ERAEXP simulation the major contribution to the transport during upwelling season is given by the undercurrent in all the domains, expect on CanCS, with values of -2.14 Sv over NBenCS (linked to Angola current), -1.64Sv over SBenCS, 1.30Sv over CalCS and -1.88 over HCS. Different the results from JRAEXP: coastal jet transport and, thus, advection of cold water for the pole, is the predominant flow over California, contributing with -0.88Sv, and over HCS it is almost comparable to the undercurrent transport (-0.8Sv) with 0.5Sv. In addition, over Benguela systems and over CanCS where, in both simulations, undercurrent transport and equatorward transport dominate respectively, JRAEXP estimates always experience grater equatorward transport and weaker undercurrent transport. In summary, as argued in several previous studies, (e.g. Capet et al. (2004), Small et al. (2015), Desbiolles et al. (2014), Marchesiello and Estrade (2010), Marchesiello et al. (2003b)), stronger ERAINT WSC associated with weak coastal wind promote stronger offshore Ekman pumping and weak coastal velocity, while weak JRA55 WSC associated with strong coastal wind generate weak Ekman Pumping and localized intense coastal upwelling. On the other hand, in terms of meridional currents, weak WSC and strong TauY at coast promote equatorward currents in the upper layer (positive differences, Figure??), and deep undercurrent, while strong WSC and weak TauY promote WSC-driven currents and thus flow upwind (consistently with Sverdrup

balance between wind stress curl and integrated meridional transport). These meridional current discrepancies, as expected, are mirrored on averaged meridional transport estimates over EBUS, highlighting interesting asymmetry on the transport structure over the water column. These discussed results clearly highlight a long-term mean response of the coastal currents to wind forcing changes, thus to investigate further this relationship at shorter timescale, we analyzed the correlation between differences in forcing and differences in coastal currents. Figure ?? shows the zero-lag correlation between differences in wind (smoothed 3 days running mean) and differences in vertical velocities as a function of latitude. Note that the correlations are computed with respect to the difference fields, namely they represent the correlations of perturbation-like changes borne by the different atmospheric forcing, rather than the full signal correlations. We consider vertical velocities integrated within the uppermost 50m depth in the first 50km off the coast as a proxy of coastal upwelling ($\triangle CU$, (Marchesiello and Estrade, 2010)), while vertically and longitudinally integrated (over the whole water column from 50km to 150km from the coast) positive vertical velocity as a proxy of Ekman pumping ($\triangle EP$). In all the domains, during the 2000-2008 upwelling season, differences in TauY at coast ($\triangle TauY$, 25 km) are highly correlated with $\triangle CU$ with values usually greater than 0.4 (95\% of statistical significance), with a maximum peak of 0.9 in the Benguela System.

Furthermore, also correlations between Ekman pumping ($\triangle EP$) and integrated WSC ($\triangle WSCit$, integrated from coast to 100km) are interestingly high and homogeneous along the coast. Correlations are significant along each EBUS, except for some specific latitude (likely due to coastline orientation) and south of 26°N in CanCS. These results highlight a local and immediate response of upwelling velocities due to wind changes, confirming TauY and WSC as qualitatively good indexes of upwelling velocities (Bakun, 1975). Nevertheless, in term of meridional currents, the clear relation in the long-term mean between wind changes and ocean currents response does not appear so evident correlating WSC and currents timesseries. Indeed, even though differences in the meridional transport over the shelf ($\triangle VSit$, from coast to 50km offshore) show relatively high correlation with $\triangle TauY$ where maxima of wind occur (CalCS, 20°S-26°S in BenCS, 30°N-32°N in CanCS and 32°S-30°S in HCS), differences in WSC ($\triangle WSCit$) do not show a significant correlation with integrated meridional transport (all the water column from coast to 200km offshore, not shown).

3.3.3 Sea Surface Temperature analysis in the EBUS

Clarified the role of wind in coastal currents, we now explore the SST variations over the studied areas. In fact, starting from the same initial condition, and thus, with an identical thermal stratification, the SST differences between ERAEXP and JRAEXP experiments underlie modifications due to dynamical and thermodynamical processes. Figures ?? (middle and bottom panels) show the mean SST bias over the study period with respect to NOAA SST for EBUS during upwelling season. In the simulation driven by JRA55 forcing, offshore BenCS and HCS warm bias (up to 2°C with ERAINT forcing) shows a reduction over the northern part of the domain, while CalCS warm bias over the southern part. Moreover, it is worth noting the different SST structure near the coast between the two simulations: a cooling of $\sim 3^{\circ}C$ is evident in the first 100 - 150 km in the JRAEXP simulation, somewhere enough excessive to turn out as cold bias (Figure ?? bottom panel).

These results, in particular the coastal cooling, suggest different processes involved in the two experiments likely triggered by the differences in winds and heat fluxes. As mentioned above, more intense coastal cooling might be caused by the coastal structure of the wind, i.e. JRA55 intense coastal wind with small wind curl generates stronger coastal upwelling and weaker offshore Ekman pumping. As a matter of fact, in JRAEXP enhanced coastal velocities determine sharper rising of colder isotherms in an area that corresponds to the coastal upwelling length (10 to 30 km, see contours in Figures?? and ??). On the other hand, the enhanced Ekman Pumping in ERAEXP is detected by a rising and a broad doming of isotherms in a strip of wind drop-off (Capet et al. (2004) and Small et al. (2015)). This is particularly evident in the BenCS and HCS sections at 200m depth. Furthermore, the discrepancy in the meridional velocity discussed in the previous section may have a role in the cooling process. Enhanced equatorward currents in the first 100km from the coast in the JRAEXP simulation promote advection of cold water from the pole along the water column either transporting directly cold water at surface or disposing it at subsurface for upwelling dynamics. It is important to underline that also variations in heat fluxes over the air-sea interface play a fundamental role on SST differences, promoting cooling through turbulent fluxes and longwave outgoing radiation and warming by shortwave and longwave incoming radiation. Thus, in order to estimate the contribution of momentum and heat fluxes on sea surface temperature at intraseasonal and interannual time scales, we implement a linear regression model between differences of SST (JRAEXP-ERAEXP) as predictand and differences in wind ($\triangle TauY$ and $\triangle WSCit$) and in downward incoming Heat Flux $(\triangle H)$ as predictors. All the differences are defined as averaged differences along the coast (from coast to 100 Km offshore and along all the latitude) and $\triangle H$ is defined as the sum of longwave and shortwave incoming radiation. To obtain intraseasonal and interannual timeseries for predictand and predictors, a Fourier transform is performed on the full timeseries. Then, for each selected timescale an inverse Fourier transform is performed by keeping the Fourier coefficients corresponding to that time scale in order to reconstruct the corresponding time series (Chavez and Messié, 2009). Expect on NBenCS at intraseasonal scale, as Table 3.2 shows, times series of reconstructed

		NBenCS		SBenCS		CanCS		CalCS		HCS	
		Coeff	%	Coeff	%	Coeff	%	Coeff	%	Coeff	%
Intraseasonal	$\triangle TauY$	-0.13	20.6	-0.63*	66.9	0.34*	38.3	0.8*	74.8	-0.40*	40.1
	$\triangle WSC$	0.16	24.6	-0.01	1.5	-0.03	3.5	-0.18	17.5	-0.28	28.4
	$\triangle H$	0.36	54.8	0.30*	31.6	0.52*	58.1	0.1	7.8	0.31*	31.5
	CORR	0.3	38	0.68*		0.73*		0.72*		0.72*	
Interannual	$\triangle TauY$	0.16	10.8	-0.73*	79.9	0.67*	46.4	0.51*	56.7	-0.62*	81.9
	$\triangle WSC$	0.81*	54.3	-0.04	4.4	-0.11	7.3	0.13*	9.3	-0.01	1.1
	$\triangle H$	0.52*	35.0	0.14	15.7	0.67*	46.2	0.29*	33.9	0.13	17.0
	CORR	0.76*		0.73*		0.76*		0.72*		0.71*	

Table 3.2: Multilinear model regression coefficients (coeff) and relative contribution on the variation of SST (weight, in percentage) of dependent variables ($\triangle WSC$, $\triangle TauY$ and $\triangle H$) to reconstruct interannual and intraseasonal differences in SST. The rows "Corr" for both interannual and intraseasonal scales indicate the correlation between times series of modelled SST and reconstructed SST. Stars (*) indicate significance of 95%. Period: 2000-2008. In bold the variables that have major contribution when the correlation is significant.

SST do significantly high correlate with modelled SST up to 0.76 in Canary an Benguela at interannual timescale. In particular, in almost all the domains, $\triangle TauY$ plays a fundamental role correlating negatively (positively) in NH (SH) with SST: the stronger the favourable upwelling winds, the colder the sea surface temperature. CalCS, HCS, and SBenSC reconstructed SST differences are explained by $\triangle TauY$ for about 75%, 40% and 67% at intraseasonal scales and, by 57%, 82%, 80% at interannual scales. Thus, SSTs variability are mostly driven by $\triangle TauY$, that promotes stronger coastal upwelling and cold advection by enhanced coastal jet. On the other hand, in CanCS both $\triangle TauY$ and $\triangle H$ equally contribute to the cooling processes: at interannual scale each of them accounts for 46% of the variability while at intraseasonal scale $\triangle H$ dominates, explaining 58% of the reconstructed variance. Finally, NBCS is the most peculiar system: SST differences are not significantly modelled by our forcing at intraseasonal time scale and interannually they are driven by WSC changing (54%). This is likely due to the fact that WSC driven Angola current (Colberg and Reason 2006) is enhanced under stronger WSC condition (ERAINT case) promoting advection of warm water from the tropics.

3.4 Discussion and Concluding remarks

In this study two reanalysis products have been employed to investigate the role of the atmospheric forcing in driving the upwelling dynamics in a climatological oriented framework. We performed two numerical experiments using a NEMO global ocean configuration at eddy-permitting resolution, sharing the same initial condition but one forced by ERA-

Interim reanalysis with 80km spatial resolution and the other by JRA55-do v1.1 with a resolution of 55Km. The analysis of the winds shows that the ERA-Interim product, when compared to QuickSCAT observations, suffers of coastal bias due to the misrepresentation of wind-drop off, too strong and too wide in cross-shore direction, whereas JRA55 product represents accurately the wind profiles characterized by weak and narrow wind-drop off and strong coastal winds (Figures ??-??-??). In all EBUS, wind stress curl and meridional winds drive offshore and inshore upwelling: weak JRA55 WSC associated with strong coastal winds generate weak Ekman pumping and intense coastal upwelling localized at the coast (Figures ??,?? and ??). The meridional currents are also sensitive to wind changes. We linked the spatial distribution of WSC and TauY to the ocean current system: the larger the upwelling-favourable curl, the more intense the poleward undercurrent and the larger the costal TauY the stronger the costal jet (Figures?? and??). In brief, solutions characterized by strong WS and weak WSC present enhanced coastal vertical velocity and strong downwind current, while sharply offshore profiles of wind stress promote longitudinally homogeneous vertical velocities and meridional currents dominated by upwind flows. These meridional flows and in turn their transport, differ also over the water column (Figures ??-??-): coastal jet current transport reaches greater depths on JRAEXP results, rather than in ERAEXP where positive transport is confined in a shallower areas. Consequently, the equivalent meridional transports (e.g equatorward and poleward) estimates in the first 300m vary and they may contribute to completely different water masses composition and nutrients. For instance, Renault et al. (2012) suggests that the shoaling of the coastal undercurrent may increase the subsurface reservoir of nutrients, stimulating primary production along the coast despite a negative effect of wind drop-off on upwelling velocities. Therefore, given the importance of the ocean dynamics on ecosystem structure and changes (EBUS Prospectus), further works with coupled ocean-biogeochemical models, regional and global, are needed in order to identify and characterize the water masses supplied to upwelling zones. Correlations between differences teach us about the rapidity of the ocean response and its localization: differences in wind are suddenly compensated by Ekman velocities (coastal upwelling and Ekman Pumping) while differences in meridional currents seem to follow the forcing changes only in restricted areas. Variability and timing of meridional currents response are different from the applied wind even though the mean response depicts evidence of relation between TauY, WSC and meridional transport (e.g. Sverdrup Balance holds in time-averaging as reported in Thomas et al. (2014)). The weak correlation might be due to latitudinally and/or temporally shifted currents response to wind modification or moreover, as Junker et al. (2015) argued, they may be related to remotely generated signals carried by Kelvin waves at the equator. As expected, these findings are reflected onto SST: enhanced coastal upwelling and equatorward advection reproduced in the JRAEXP simulation lead to a clear cooling in the first 100km in all

the domains, generally damping the warm bias that is evident in the ocean driven by ERAINT. This is particularly evident around capes and wind maxima, where upwelling dynamics dominates (Jr et al. (2009); Kirkman et al. (2016)). A linear regression analysis shows that the contribution of the wind on sea surface temperature differences at interannual and intraseasonal time scales is always greater than the contribution due to incoming heat fluxes, explaining at least for the 40% of its variation. The only exception is the CanCS where at intraseasonal scale the heat flux contribution is the largest. Reconstructing the intraseasonal variability of the SST at NBenCS is more challenging since this area is driven by a complex dynamics, characterized by abrupt changes of wind during time and by the front between the Angola and Benguela Currents (ABF) whose seasonal variation is usually not well represented in models (Xu et al., 2014). Therefore, more sophisticated relationships than multi-linear regression shall be considered in the future for this area. In light of the crucial role of the wind, it might be argued that the cooling and the equatorward currents structure may be considered excessive if important changes of the wind occur near the coast (within 25 km) promoting sharper wind drop-off (e.g strong WSC and weak TauY at coast) and also the resolution of the ocean model could be a source of error, too coarse to properly resolve the upwelling dynamics scale (20 km). Nevertheless, the main objective here was to provide a process-oriented study in a climate and global perspective framework, and therefore the choice of the 1/4° model resolution can be considered adequate to investigate the ocean response to the considered forcing. In summary, the four wind-driven upwelling areas have similar spatial patterns of wind stress and wind stress curl, which drive similar current systems in spite of otherwise significant hydrographic and bathymetric differences. Such similarity appears to call for a common climatological response of the regional oceanic circulation in the EBUS primarily sensitive to near-shore (200Km) wind drop-off and coastal wind. All EBUS present a coherent response to different structure of wind (except for the area south of 26°N in Canary System) and our results are in line with observational studies (Junker et al. (2015), Fennel et al. (2012)) and previous model studies (e.g. Capet et al. (2004), Small et al. (2015), Desbiolles et al. (2014), Marchesiello and Estrade (2010), Marchesiello et al. (2003b)), confirming the importance of the wind stress nearshore structure on upwelling dynamics and in turn on its ecosystem. The results and the quality of JRA55do v.1.1 wind encourage further climate oriented studies on wind forcing over EBUS. For instance, the impact of resolution in coastal processes could be further assessed enhancing wind forcing resolution up to ocean model using statistical downscaling method (Goubanova et al. (2011), Cambon et al. (2013b)). Moreover, downscaled wind forcing could be used for investigating further the temperature and meridional ocean currents structure in EBUS, particularly the distinction between equatorward currents driven by equatorward wind and poleward currents driven by cyclonic wind curl is still an open issue together with the understanding of EBUS

dynamics under climate change (Bakun (1990), Rykaczewski et al. (2015a)). Furthermore, the interannual to decadal variability of EBUS, not debated in this work, and its link with large-scale climate modes will be the subject of Chapter 4, in order to shed some light on the observed and modelled decadal scale changes in upwelling (Tim et al. (2015), Sydeman et al. (2014b)) and in ecosystem structure (Peterson and Schwing (2003), ?, Roesler (1987), Rebstock (2003)).

Chapter 4

Interannual to decadal Climate Variability within and across the major Eastern Boundary Upwelling Systems

4.1 Introduction

The Eastern Boundary Upwelling Systems are among the most productive marine ecosystems supplying up to 20% of the global fish catches even though they cover less then 3% of the global ocean (Sydeman et al. (2014a), Pauly and Christensen (1995)). Surface alongshore winds, in combination with the Coriolis effect, force surface water offshore, through Ekman Transport and Ekman pumping, thereby driving deep, nutrient-rich waters to the sunlit surface layer, stimulating blooms of phytoplankton, the base of the oceanic food web. Recent studies documented trends (Tim et al. (2015), Wang et al. (2015), Sydeman et al. (2014a)) and decadal scale changes in EBUS ecosystem structures (Lehodey et al. (2006), Parrish et al. (2000)). One of the most compelling examples is the so-called Regime Problem: sardines and anchovies regimes appear to fluctuate, since the early 1980s, with a 20 to 30 years period driven by climate processes (Lluch-Belda et al. (1989) and LLUCH-BELDA et al. (1992)). Thus, understanding the low-frequency drivers and monitoring changes across EBUS is of great importance. Each of the EBUS covers a large range of latitudes, and has substantial spatial and temporal heterogeneity in its physical characteristics. In particular, the upwelling intensity is uniformly distributed across seasons in regions closer to the Equator (Messié et al., 2009), while the upwelling variability is highly seasonal at temperate latitudes, with generally higher intensity of upwelling in boreal (austral) spring and summer in NH (SH) domains. Beside the well-known seasonal variability mainly driven by the wind stress, the low-frequency modulation of the upwelling

seasonal cycle and its drivers are not established yet. The coastal trapped waves and the eddy activity may play an important role. The former, generated by the alongshore pressure gradient due to the persistent equatorward winds, influences the stratification (Pietri et al., 2014), while the latter impacts the offshore transport (Combes et al. (2013) and Cessi and Wolfe (2009)).

Identifying large-scale drivers is also important to understand the long-term trend of the EBUS as a response of anthropogenic climate change. Bakun (1990) observed a general trend of the upwelling intensification related to the wind intensity increase. Later on, Bakun et al. (2010) hypothesized an increase in upwelling-favorable winds due to intensification of the continental-oceanic pressure gradient under global warming. A more recent hypothesis suggests that a poleward shift of the oceanic high-pressure system (Rykaczewski et al. (2015b), Wang et al. (2015)) could stimulate latitude-dependent changes in the magnitude and timing of upwelling winds. Beside the different mechanism proposed, both theories agree on the intensification of upwelling-favourable winds at least in the poleward part of the systems. A considerable amount of literature has emerged since the original hypothesis, showing data for and against the upwelling intensification mechanism within the four main EBUS. Recently, García-Reyes et al. (2015) proposed a synthesis on wind stress trends over EBUS and they argued that climate models and, with low confidence, observational data suggest increased (decreased) trends in upwelling-favorable winds in the poleward (equatorward) regions of the EBUS by changes in the positioning of the oceanic high-pressure systems, rather than by deepening of the continental low-pressure systems. Despite the overall agreement, a lot of discrepancies are, anyway, reported in this review and some others have been published after. For instance, Narayan et al. (2010) depicted decreasing trends in California; Dewitte et al. (2012), Tim et al. (2015) do not reported any trends in the Peru and Benguela systems respectively, while Pardo et al. (2011) and Sydeman et al. (2014a) showed a decreasing trend in the Canary systems, especially along Iberian coast. Although there is scientific consensus on the future of upwelling-favourable winds, there is low confidence regarding the future of coastal temperature and biogeochemistry in all the EBUS (Mendelssohn and Schwing (2002), Arístegui et al. (2009); Belkin (2009); Demarcq (2009); Lebassi et al. (2009); García-Reves and Largier (2010); Rouault et al. (2010); Gutiérrez et al. (2011); Sydeman et al. (2014b)b; Salvanes et al. (2015)). This is due to uncertainty in the countervailing responses to increased upwelling-favourable wind and coastal warming. In fact, the latter increases water stratification and could render upwelling less effective in lifting nutrient-rich deep waters into the photic zone (Di Lorenzo et al., 2005). Results of the trend analysis do highly depend on the type of dataset used, the temporal coverage, and variable considered as upwelling index (Tim et al. (2015), Sydeman et al. (2014a), García-Reyes et al. (2015)). Therefore, the consensus about EBUS future changes, in particular the impact on ecosystems (e.g. nutrients), has not yet been reached.

From a larger-scale climatic perspective, climate modes seem to exert some control on the interannual to decadal variability of upwelling, further complicating the extraction of long-term trends from observational records and model simulations (García-Reyes et al., 2015). Many of the most significant upwelling modifications in EBUS, particularly in the Pacific Ocean, have been attributed to large-scale, ocean-atmosphere processes (Jacox et al., 2015). ENSO is the leading mode of variability of the Humboldt System (Minobe and Mantua, 1999), while decadal oscillations like Pacific Decadal Oscillation (PDO), and the North Pacific Gyre Oscillation (NPGO) are linked to California System variability (Chhak and Di Lorenzo (2007); Di Lorenzo et al. (2008); Jacox et al. (2015)). Different are the finding for the domains in the Atlantic sector. The Benguela System is poorly affected by basin-scale thermocline perturbations (Atlantic El Ni \tilde{n} o), but highly affected by small-scale local physical variability (Chavez and Messié, 2009). Nevertheless, Hagen et al. (2001) mentioned a possible influence of the Quasi-Biennial Oscillation (QBO), a mode of variability that describes quasi-oscillations of low stratospheric winds, and Antarctic Oscillation (AAO), and, according to other studies (e.g. Dufois and Rouault (2012)), ENSO signal could be of great importance. Over Canary/Iberian Current System, several studies report a large influence of the North Atlantic Oscillation (NAO) and the Atlantic Multidecadal Oscillation (AMO) on upwelling magnitudes and interannual-to-decadal variability (Cropper et al. (2014), Narayan et al. (2010), Pardo et al. (2011)).

In addition to the backdrop of these competing findings, there are no reported studies about an interannual-to-decadal shared variability across the EBUS, despite the well-known shared low-frequency variability between the northern and the southern Pacific Ocean, mainly due to ENSO. The EBUS have similar spatio-temporal patterns of wind stresses and ocean currents at climatological timescales (see Chapter 3), but commonalities and dissimilarities are not yet established and understood over interannual-to-decadal timescale (EBUS Prospectus 2018). Therefore, the overriding aim of this work is to shed some light on the low frequency variability of EBUS. In particular, the objectives of this study are to:

- 1. establish if low-frequency variations of the tracers are the result of low-frequency modulations of the seasonal cycle;
- 2. identify the forcing dynamics that control low-frequency modulations of the seasonal cycle;
- 3. evaluate and discuss significant upwelling trends;
- 4. identify connection between upwelling index of each EBUS and climate modes;
- 5. understand the extent to which the low-frequency variability is shared across EBUS and identify its large-scale dominant drivers.

For these purposes, we analyzed the low frequency variability of modelled upwelling using a NEMO global ocean hindcast simulation covering the past six decades. In this simulation, the ocean is driven by a new atmospheric forcing product (with a resolution of 25 km) obtained through a statistical downscaling and merger of the large-scale wind structures from JRA55do-v1.1 (Tsujino et al., 2018) with the high resolution QuikSCAT winds. Furthermore, passive tracers have been used in the ocean model to highlight features of the coastal subsurface waters and helps in identifying a proxy for coastal upwelling strength, following the approach by Combes et al. (2013) who studied the upwelling and cross-shelf transport variability in the California Current System and Humboldt Current System. Moreover, the advantage of using a global model, instead of a regional configuration applied on a single EBUS, allows us to compare and identify commonalities and dissimilarities among EBUS dynamics and drivers. The paper has the following structure. Data and methods are described in Section 2, followed by a basic validation of the model output regarding the ocean dynamics. The results are presented in the sections 3 and 4. The former presents the upwelling seasonal cycle and its low-frequency modulation and its drivers; the latter the correlation with climate modes and shared interannual-to-decadal variability across EBUS. Finally, these results are discussed in Section 5, highlighting the key conclusions.

4.2 Data and methods

4.2.1 Ocean model setup

Description of NEMO global ocean model configuration

The variability of EBUS is investigated in a numerical study based on the state-of-theart modelling system NEMO (version 3.6, Madec (2015)), a three dimensional, free-surface, hydrostatic, primitive-equation global ocean general circulation model coupled with the Louvain-la-Neuve Sea Ice Model, LIM2 (Bouillon et al., 2009). Our configuration employs the global ORCA025 tripolar grid (Madec and Imbard (1996)) with horizontal resolution of $1/4^{\circ}$ ($\sim 27.75km$) at the Equator, increasing with latitudes, e.g. $\sim 14km$ at 60°N or 60°S. The vertical grid has 75 levels, whose spacing increases with a double hyperbolic tangent function of depth from 1m near the surface to $\sim 200m$ at the bottom, with a partial step representation of the bottom topography (Bernard et al., 2006). The model bathymetry is a combination of the ETOPO1 data (Amante and Eakins, 2009) used in the deep ocean and GEBCO (IOC, IHO and BODC, 2003) in coastal regions. Tracer advection uses a total variance dissipation (TVD) scheme Zalesak (1979). Laplacian lateral tracer mixing is along isoneutral surfaces with a coefficient of 300 m^2s_{-1} . The vertical mixing of tracers and momentum is parameterized using the turbulent kinetic energy (TKE) scheme. The freshwater input to the ocean is derived as monthly climatology from the global river flow and continental discharge data set by Dai et al. (2009) together with the Antarctic coastal freshwater discharge estimated by Jacobs et al. (1996)).

Initialization and atmospheric forcing: statistical downscaling of JRA55do with QuikSCAT

To study the EBUS variability, we performed an ocean model simulation (hereinafter TRD55). The simulation covers a period from 1958 to 2015, and the initial conditions are provided in December 1957 by the December 2015 of an existing ocean simulation forced by JRA55dov1.1 reanalysis (presented in Tsujino et al. (2018)). The extreme sensitivity of EBUS to the specific structure of the wind reported in several studies (Desbiolles et al. (2014), Capet et al. (2004), Small et al. (2015), and Pickett and Paduan (2003)) encouraged us to develop a new high-resolution wind dataset, based on observational estimates to force the ocean dynamics in the TRD55 experiment. We compute a statistical downscaling of the wind over EBUS using QuickSCAT wind retrievals, following the method developed in Goubanova et al. (2011). This technique provides an important correction of coastal wind patterns off EBUS thanks to the QuikSCAT accuracy (Garreaud and Muñoz (2005); Dewitte et al. (2011)). In JRA55, even though with an evident improvement from ERAInterim (Chapter 3), the representation of wind drop-off is still an open issue that impacts Ekman pumping, coastal upwelling (Bakun, 1990) and alongshore transport (Marchesiello et al., 2003a). In addition, the JRA55 spatial resolution is still too coarse to resolve upwelling dynamics, usually confined in 30km from the coast. The main idea of statistical downscaling consists in building a statistical relationship between local/regional variables (predictand) and large-scale climate characteristics (predictors) for the period where predictand, usually observations, are available. This relationship is then applied to predictors into the past or the future. In this way, it is possible to correct the predictor fields also when observations are not available. As presented in Goubanova et al. (2011), the statistical relationship is based on a multiple linear regression. The predictand is the near-surface wind measured by QuikSCAT scatterometer (gridded product from IFRE-MER: 0.25° x 0.25° spatial resolution, 1-day temporal resolution from 2000 to 2008). The large-scale predictors, covering the QuikSCAT period, are the sea level pressure (SLP) and near-surface wind fields from JRA55 data. The statistical relations between predictand and predictors were then used to downscale JRA55 surface winds for the period 1958-2015 obtaining a new high-resolution dataset (same resolution of predictand, 25km), corrected by observations. (See Appendix A, for details on downscaling method) To drive our ocean, the other atmospheric variables, turbulent variables (temperature and specific humidity at 2 m), radiative fluxes and precipitation, are provided 3 hourly by the JRA55 reanalysis.

Passive tracer set up

Aim of this study is to identify the water masses at subsurface (usually rich in nutrients) that could reach the surface by vertical advection. Therefore, following the approach of Combes et al. (2013) and Combes et al. (2015), we introduce passive tracers in each EBUS at subsurface (150-300m). In the NEMO model, they are calculated by a passive tracer advection-diffusion equation with a decay term:

$$\frac{\partial Tr}{\partial t} = -\vec{u} + A_H \nabla_H^2 Tr + \frac{\partial}{\partial z} (A_v \frac{\partial Tr}{\partial z}) + \tau (Tr - T_0)$$
(4.1)

where Tr is the passive tracer concentration, A_H is the horizontal diffusivity, A_V is the vertical diffusivity, T_0 is the restoring term that controls the continuous source of tracer at sub-surface, \vec{u} is the velocity field, and τ is the decay timescale set to 6 months (needed to avoid an infinite growth of passive tracer concentrations within the interior of the model domain interior). To characterize the upwelling of subsurface nutrient-rich water, we choose the source term (To) such that the passive tracer (Tr) is set to 1 in the coastal areas over the regions illustrated by the white rectangles in Figures ??-?? (from the coast to 50 km offshore), and in the subsurface from 150 to 250 m depth. Due to the fact that EBUS are temporally and spatially heterogeneous environment (Wooster, 1963) and are usually divided by latitude in different upwelling regimes (See Chapter 2), we divided each EBUS in a northern and a southern part in which we injected two independent tracers. In particular, the Benguela system is divided in two areas at 26°S, north of Lüderitz (see white square Figure ??), hereinafter Northern Benguela (15°S-25°S, NBenCS) and Southern Benguela (26°S-34°S, SBenCS). Note the difference with Chapter 3 for NBenCS and SBenCS. The California domain is instead partitioned at Cape Mendocino (34°S) in Northern California System (34°S-41°S, NCalCS) and Baja California (34°S-27°S, SCalCS). The subdivision is even more obvious for Canary and Humboldt/Peru System. In the former, tracers are inhected over the Iberian Peninsula (40°N-44°N, NCanCS) and over the Moroccan Sector (20°N-28°N, SCanCS), in the latter along the Peruvian coast (5°S-15°S, NHCS) and along Chilean coast (25°S-35°S, SHCS). In addition to other published works on EBUS variability that inferred upwelling using the coastal wind stress, the SST differences between coast and offshore, or the vertical mass transport, here we consider the concentration of tracers found at the surface a measure of upwelling. In particular, we define an upwelling index (UI) as the monthly tracer concentration at surface, from the coast to 100 km offshore and at the latitude where the tracer is released (see white square Figures ??-??). Moreover, we defined a second index as the low-frequency modulation of the upwelling seasonal cycle (UI_{slw}) that is the projection of the seasonal tracer concentration at surface into its seasonal variation (see section 3.1 for a detailed description of this index).

4.2.2 Indices and observation

Upwelling indices

In this work we consider the concentration of each tracer found at the surface a measure of upwelling. In particular, we define:

- monthly upwelling index (UI): monthly tracer concentration at surface, from coast to 150 km offshore and along the latitude where the tracer is released (see white boxes in Figures ??-??);
- annual upwelling index (UI_a) : defined as UI but with annual mean;
- low-frequency modulation of the upwelling seasonal cycle (UI_{slw}) : the projection of the seasonal tracer concentration at surface (from coast to 150 km offshore and along the latitude where the tracer is released) into its seasonal variation:

$$F(t)_{seas} = F(x, y)_{seas} * F(x, y, t)_{seas}$$

$$(4.2)$$

where F indicate either the response variable (tracer concentration) or the forcing; x and y are the spatial coordinates; t is the time. Seas subscripts identify the season where upwelling is maximum (see previous section).

Drivers indices

To investigate the drivers of upwelling we consider alongshore wind stress, wind stress curl and stratification as forcing. We consider:

- alongshore wind stress index (WS): the projection of the seasonal alongshore wind stress (from coast to 50 km offshore and along the latitude where the tracer is released) into its seasonal variation. Alongshore wind stress is calculated rotating the u and v component of wind stress to shoreline direction;
- wind stress curl index (WSC): the projection of the seasonal tracer concentration at surface (from coast to 150 km offshore and along the latitude where the tracer is released) into its seasonal variation.
- Stratification index or Remote Forcing Index (RFI): the depth variation of a representative isopycnal below the mix layer depth (usually around 10m) in time (see Figures 2 and 3 for isopycnals definition). In order to consider the stratification as an external driver of upwelling in our statistical model, we first analyzed the net heat flux (Qnet). Due to the nature of these areas and the complex air-sea feedback, Qnet results to be intensified toward the ocean during upwelling. As a matter of fact, in NHCS (Figure ??), upwelling index and Qnet are related by positive correlation

(Figure ??a), while SST and Qnet by negative correlation (Figure ??b). As argued in Jacox et al. (2015), the surface cooling associated with the upwelling actually facilitates upper ocean heating by intensifying the air-sea temperature gradient near the coast. For this reason, we calculated a new index, namely Remote Forcing Index (RFI), computed as the depth variation of a representative isopycnal below the mixed layer depth (usually at $\sim 10m$) in time (see caption of Figure ?? for isopycnals definition). RFI is a measure of stratification and of the passage of coastal trapped waves.

It is worth noting that the times series resulted from the projection, as a modulation of the mean field, have positive sign even though, for instance, the sign of the wind stress field is negative (e.g. NH systems).

Climate indices

The upwelling indices are not only correlated with the atmospheric variables but also with climate indices. The influence of the Multivariate ENSO Index (MEI; Wolter and Timlin (2011)), the Tropical Pacific Decadal Variability (TPDV, 0° E - 20°E, 3°N-3°S; Choi et al. (2013)), the Pacific Decadal Oscillation (PDO, Mantua and Hare (2002)), the North Pacific Gyre Oscillation (NPGO, Di Lorenzo et al. (2008)), the Antarctic Oscillation (AAO; Marshall and Radko (2003)), the North Atlantic Oscillation (NAO, Barnston and Livezey (1987)) are investigated. Moreover we also consider the impact of the Atlantic Meridional Mode (AMM; Chiang and Vimont, 2004), the Pacific Meridional Mode (PMM; Chiang and Vimont (2004)), the Atlantic Meridional Oscillation (AMO; Enfield et al. (2001)), the Quasi-Biennial Oscillation (QBO; Labitzke and Van Loon (1992)) and the Tropical Atlantic (ATL-3, 20°W-0°E, 3°N-3°S; Rodríguez-Fonseca et al. (2009)). The TPDV and ATL-3 values are calculated from the NOAA SST. To analyse the statistical significance of the long-term trends of the upwelling indices and the linear correlations between them and climate modes, a two-sided significance level of p = 0.05 is adopted. In the Results section we take advantage of projection to extract climate modes variability over specified areas. For instance, we isolate the AAO variability over the South Pacific domain projecting AAO correction pattern over the South Pacific domain onto NOAA SSTa (SAAO-P, see Supplementary Figure S3b). We performed the same for South Atlantic region (SAAO-A, see Supplementary Figure S3c).

Gridded observational data

We use monthly mean sea level pressure (SLP) fields obtained from the National Centers for Environmenta Prediction-National Center for Atmospheric Research (hereinafter NCAR) atmospheric reanalysis (Kalnay et al., 1996), available on a global 2.5° x 2.5° hor-

izontal grid. Furthermore, we use the National Oceanic and Atmospheric Administration Extended Reconstruction SST, version 3 (hereinafter NOAA SST) product (Smith and Reynolds, 2005), it consists of monthly mean values at 2° x 2° horizontal grid from 1854 to the present. We restrict the period of record to 1958-2015 to match the model results. Note that in this Chapter NOAA SST refers to global dataset provided by Smith and Reynolds (2005), while in Chapter 2 and 3 NOAA SST refers to Reynolds et al. (2007).

Throughout the text and figures, the significance of correlations is estimated based on the probability density function (PDF) of the cross-correlation coefficients between 2 time series s1 and s2. The PDF is built by computing the correlation of 5000 random pairs of time series that possess the same autocorrelation of s1 and s2. Moreover, the significance of the trends is estimate based on the PDF of the trend coefficients.

4.3 Results

4.3.1 Model Validation

We first use observed dataset to evaluate the performance of TRD55 to simulate ocean variability. In Figure ??, we compare the standard deviation of the modelled sea surface height anomaly (SSHa) and its mean value against the satellite altimetry data from AVISO over the 1993-2015 period (Figure ??). In general, the TRD55 standard deviation underestimates the observed SSHa, while the amplitude and spatial structure of the modelled mean SSHa compares relatively well with AVISO. Maxima are located over the Indian Ocean and along the western boundaries of the ocean, while minima are over the Southern Ocean and along the eastern boundaries. To validate the coastal variability of the model solutions, Figure?? presents a comparison of time series of the modelled and observed SSHa averaged over EBUS domains (red (blue) squares in Figure?? for northern (southern) part of each EBUS). The model coastal SSHa explains a significant fraction of the sea level variance in all the EBUS. Major discrepancies are reported over Atlantic systems. Off Benguela and, in particular, off the Iberian coast, TDR55 poorly simulates the observed SSHa, likely due to the high variability induced by Angulas current in Benguela Systems (Chavez and Messié, 2009), and to the extension of Gulf stream in Western Iberian Peninsula (Palter, 2015). Different are the cases over the Pacific Ocean, where correlations between modelled and observed variability reach values of about 0.9. For instance, the strong positive anomalies during the warm ENSO events of 1982 and 1998 (El Niño years) are perfectly depicted either in California and in Peru systems.

4.3.2 Upwelling Seasonal Cycle

The mean seasonal variabilities of coastal upwelling (UI, section 2.1.3) are summarized in Figure??. Canary and California areas experience the maximum upwelling activities during boreal spring/summer, while Benguela and Peru systems during boreal autumn/winter. We find that the amplitude of the seasonal cycles varies substantially across the different systems. In the northern hemisphere, the NCanCS and NCalCS show the most pronounced seasonal cycle with maximum in April-May-June (AMJ) and May-June-July (MJJ), while SCalCS and SCanCS systems exhibit a weak seasonality. In the southern hemisphere, upwelling is enhanced during December-January-February (DJF) in SBenCS, during November-December-January (NDJ) along SHCS, and in September-October-November (SON) in NBenCS and along NHCS. To assess the realism of the model in simulating the upwelling seasonal cycles, we compared the UI with the AVISO seasonal cycle in the areas of interest (blue line in the panels e of Figures ??-??). The signals show an anti-phase relation in all the domains: the more intense the coastal upwelling (positive tracer anomalies), the colder the surface water and the lower the sea surface height (negative SSH anomalies), and vice versa. Furthermore, the upwelling seasonal cycles are in phase (anti-phased) with the seasonal cycle of meridional wind stress over the Southern (Northern) Hemisphere domains (Figures??-?? panels b), a result consistent with the theories of the response of seasonal coastal upwelling to alongshore wind stresses changes (Bakun, 1990). The only exception is along the Northern Peru coast in which UI peaks right after the boreal summer wind maxima (JJA), namely during boreal fall (SON, Figure ?? top panels e). Nevertheless, despite the meridional wind stress, the eddy activity and the wind stress curl are enhanced during boreal fall, likely promoting advection of tracer offshore and Ekman Pumping respectively (compare Figure ?? top panels with Figure ?? bottom panels). Another discrepancy with wind maxima is detected over NBenCS (Figure??): boreal spring wind maxima are not reflected in the tracer concentration at surface. Figure ?? shows the mean salinity and temperature during the seasons. During the first two quarter of the year (boreal winter, DJF, and boreal spring, MAM) the intrusion of warm and salty water is evident from the Angola current in the subsurface. This warm/salty water enhances stratification and traps the tracer in the subsurface by significantly weakening upwelling during boreal spring. Consistent with this picture, Shannon et al. (1987) and Rouault et al. (2007) assert that Cape Frio (17°S, Northern Benguela) is, in terms of wind, a centre of a potential upwelling comparable with the Lüderitz area (27°S, Southern Benguela), although this is not always evident in the SST/tracer distribution, as it is superficial and relatively warm water that upwells. The seasonal concentration patterns of the tracers (Figures ??-?? contours panels a), computed over the main seasonal described above, are localized nearby the maximum of the wind stress (panels c) and are stretched along the direction of the mean circulation (panels d), poleward in Northern Benguela System (around 16°S) and equatorward elsewhere. Moreover, cyclonic wind stress curl (Figure ??-?? contours in panels c, negative (positive) in NH (SH) domains) also promotes upwelling. Signature of upwelled water is evident in the coastal areas from pattern of sea surface temperature and net heat flux, in fact the former shows cold temperature and the latter positive heat fluxes during upwelling season (Figures ??-?? panels b). Particular is the case of SCalCS (Figure ??, bottom panel a) with a more uniform coastal upwelling along the entire coast, outside the areas of permanent tracer source, indicating that, in addition to a southern upwelling, the poleward alongshore transport of southern water masses is an important exchange mechanism between the southern and central California.

4.3.3 Drivers and trends of low frequency modulation of upwelling

Once the predominant seasonality is defined in each domain, we analyzed the low frequency modulation of upwelling seasonal cycle in order to identify its main drivers. To estimate the contribution of the forcing field to the long-term trend during the upwelling season, we set up a linear regression model between UI_{slw} as predictand and the time series of forcing forcing (e.g. alongshore wind stress, wind stress curl and RFI) as predictors (see Data and Methods for indices definition):

$$UI_{slw} = \alpha W S_{slw} + \beta W S C_{slw} + \gamma R F I \tag{4.3}$$

where WS_{slw} , WSC_{slw} , RFI are the low-frequency modulation of meridional wind stress, wind stress curl and stratification respectively; α, β, γ the regression coefficients.

Figures ?? and ?? display the results of the regression and Table 4.1 reports the coefficients for each forcing. The reconstructed tracer signals (Trec, red lines) are in good agreement with the tracer modulation (UI_{slw}) , explaining about the 70% of the variance in all the domains (see Corr correlation coefficient in each subplot). Thus, UI_{slw} is the result of low-frequency modulations of the forcing seasonal cycle, and moreover the high correlations of UI_{slw} with low frequency variation of tracers in all domains (e.g annual mean, last row of 4.1) indicate that the modulation of the upwelling seasonal cycle dominates the upwelling interannual variability. The low frequency variabilities of upwelling seasonal cycle of Benguela systems is completely explain by the fluctuation of wind stress, accounting for 72%, 70% of the modelled UI_{slw} , respectively. The stratification and, also, the passage of coastal-trapped waves together with the wind stress, in minor contribution, are the major drivers of the other regions, modulating the intensity of the subsurface upwelled water at interannual timescale. In particular, as negative correlation coefficients indicates in Table 4.1, the deeper the isopycnal the weaker the upwelling intensity. RFI explains about 55%

of the modelled upwelling modulation in Canary Systems, about 60% in California Systems and up to 76% in Humboldt Systems. The only region where the wind stress curl modulation and thus Ekman pumping seems to play a role is over NCanCS, explaining 20% of the variance. The remain variabilities of UIslw not explained by the main drivers, less than 30% over the all domains, are likely due to the horizontal advection and to the eddy activities (Cessi and Wolfe, 2009). In particular, that can be the case of SCalCS where poleward flow (e.g undercurrent) and deep cyclonic eddy transport surface and subsurface water masses to the north (Combes et al., 2013). Moreover, Benguela systems and Canary Systems show significant trends: positive for Benguela and negative for Canary (Table 4.1, last row). The computed trends display a significant overall increasing in Benguela and decreasing in Canary systems. In both cases they are driven by wind changes, even though part of Canary tendency appears to be related to RFI/stratification. Our results support Bakun Hypothesis just over Benguela Systems, while do not support it for the other EBUS. Furthermore, trends coherency between northern and southern domains of Benguela and Canary systems do not support either the theory on the poleward displacement of high pressure-systems that should favourite upwelling poleward (Rykaczewski et al., 2015a). Having described the forcing of the low-frequency seasonal variability of the upwelling and its trends, we now explore if the low frequency variability of SST during upwelling season (SST_{slw}) is driven by upwelling. The correlation between UI_{slw} and SST_{slw} (shown in 4.1) is high in all domains except in NBenCS (correlation coefficient -0.05). Nevertheless, this result is just an artifact of computing SST mean in the area between 15°S and 25°S. Indeed, as Figure ?? depicts, the spatial correlation between the UI_{slw} and the SST_{slw} results positive north 20°S and negative elsewhere. Near Cape Frio, where upwelling is completely inhibited by stratification, as previously argued, the concentration of the tracer is regulated by advection through warm and salty Angola current (positive correlation), while upwelling regulates SST further south, where upwelling actually occurs, bringing cold water at the ocean surface (negative correlation). In summary, the reported results highlighted the uniqueness of each EBUS in their low-frequency variability. In fact, they are driven by different processes, and present contrasting trends (if not insignificant).

4.4 Correlation with climate modes and Coherent lowfrequency variability across EBUS

By means of the statistics of passive tracer concentration, we study the link between upwelling and the modes of large-scale climate variability. Here, the goals are: (1) to evaluate, for each EBUS, the correlation between low-frequency variability of upwelling index and climate modes; (2) to understand the extent to which the low-frequency variable.

	NBei	nCS	SBei	nCS	NCa	nCS	SCar	nCS	NCa	lCS	SCa	lCS	NH	CS	SHO	CS
	Coeff	%														
WS	0.93	72.6	0.63	70.3	0.58	28.5	0.36	30.4	0.31	29.2	0.25	26.0	0.06	6.4	0.34	34.2
WSC	-0.18	14.5	0.09	11.0	0.30	20.2	0.15	11.8	-0.04	4.3	0.15	16.0	0.17	16.7	0.01	4.0
RFI	-0.16	12.8	0.17	18.8	-0.63	51.2	-0.69	57.8	-0.71	66.5	-0.57	58.1	-0.82	76.9	-0.62	61.8
UI_{slw} - SST_{slw}	-0.0	05	-0.	.4	-0.	51	-0.'	77	-0.	77	-0.0	69	-0.8	82	-0.	52
UI_{slw} - UI_a	0.9	94	0.7	78	0.9)1	0.8	38	0.9	94	0.9	95	0.8	37	0.7	79
UI_{slw} Trend	0.0	5*	0.0	5*	-0.0	4*	-0.0	4*	0.00	004	0.0)1	-0.0	01	-0.0	01

Table 4.1: Multi-linear regression coefficient and contribution in percentage of predictors (WS, WSC, RFI), from first to third rows. Correlation between low frequency modulation of upwelling seasonal cycle (UI_{slw}) and seasonal SST_{slw}, or long-term modulation of upwelling (e.g. annual mean, Tra). Last row reported upwelling index UI_{slw} trends in [std/year]. Stars (*) indicate significant values.

ability is shared across EBUS; (3) to identify the large scale dominant drivers of this shared variability.

4.4.1 Correlation with climate modes

To achieve these objectives, we first assess the connection between upwelling index (UI) of each EBUS and climate modes. The correlation of UI with the following climate modes, ENSO (MEI), AAO, PMM, AMM, AMO, NAO, PDO, NPGO, TPDV, QBO and ATL-3, are investigated. Table 4.2 summarizes the main findings. We find significant correlation between the upwelling indices of California Systems and the PMM, PDO, NPGO, MEI and TPDV climate modes. The PMM negatively correlates with upwelling (-0.30 and -0.34 correlation coefficients with NCalCS and SCalCS, respectively). In fact, this mode, which is mostly a stochastic phenomenon that evolves from wind-evaporation-SST feedback (WES) over the Pacific Ocean, is characterized, in its positive phase, by warm SST that weakens trade winds and equatorward winds along the Northen Pacific coasts (Stuecker, 2018). PDO and NPGO, as correlation coefficients show, control part of decadal modulation of the California upwelling. Indeed, they are strongly related to PMM low-frequency components (Stuecker, 2018) and, moreover, they are forced by the Aleutian low (a semipermanent low-pressure system located near the Aleutian Islands) and the North Pacific Oscillation that act on wind stress field in the Northern Pacific. As pointed out in Chhak and Di Lorenzo (2007) and in Di Lorenzo et al. (2008), the PDO signal has more influence over NCalCS (-0.45 correlation coefficient), while the NPGO over SCalCS (0.45 correlation coefficient). Finally, MEI shows significant correlation of about -0.38 with the California systems. In fact, strong ENSO events impact the biochemical response to upwelling through modulation of both the seasonal thermocline depth (Chavez et al., 2002) and the strength of nearshore upwelling-favorable winds (Schwing et al. (2002); Jacox et al. (2015)). As

	NBenCS	SBenCS	NCanCS	SCanCS	NCalCS	SCalCS	NHCS	SHCS
AMO	0.13	0.11	-0.31*	-0.37*	-0.10	-0.08	0.10	-0.04
AMM	0.25	0.22	-0.37*	-0.39*	-0.13	-0.06	0.09	-0.02
MEI	0.02	-0.04	-0.05	-0.11	-0.37*	-0.38*	-0.60*	-0.50*
PDO	-0.11	0.02	-0.09	-0.02	-0.45*	-0.38*	-0.32*	-0.33*
NPGO	0.10	-0.06	-0.11	-0.03	0.30*	0.45*	0.19	0.21
TPDV	0.03	0.08	0.04	0.10	0.31*	0.32*	0.64*	0.48*
AAO	0.20*	0.28*	-0.12	-0.03	0.01	0.04	0.10	0.11
PMM	-0.08	-0.04	0.04	-0.08	-0.30*	-0.34*	0.15	0.01
QBO	-0.02	0.10	-0.02	0.02	0.02	0.04	-0.04	-0.07
NAO	0.03	0.11	0.13*	0.17*	0.03	-0.10*	0.03	0.01
ATL-3	-0.25*	-0.07	-0.06	-0.02	0.06	0.15	-0.02	0.11

Table 4.2: Correlation coefficients of the upwelling indices derived from the tracer concentration of the TRD55 simulation of EBUS with AMO, AMM, MEI, PDO, NPGO, TPDV, AAO, PMM, QBO, and NAO. Significant correlations are highlighted by stars (*). All time-series linearly detrended beforehand.

expected, time series of Peru upwelling are completely dominated by ENSO and its low frequency modulation (TPDV), showing -0.59/0.64 for the northern region and -0.5/0.48 for the southern region. As for California Systems, during El Nino conditions, a deep thermocline and anomalously weak equatorward winds reduce the efficacy of upwelling for delivering nutrients to the euphotic zone (Jacox et al., 2015).

In the Atlantic Ocean, our analysis shows that AAO climate mode could influence upwelling in both Benguela systems, while ATL-3 could, at most, have affected NBenCS. Presumably, AAO, tends to reinforce upwelling favorable winds in this region, regulating the strength of the circumpolar westerly flow (Jones and Widmann, 2004), while ATL-3, the equivalent ENSO on Atlantic, weakens the upwelling-favorable winds during its positive phase, acting on trades winds (Tim et al., 2015). Lastly, Canary systems are significantly influenced by AMM/AMO, with significant correlation coefficients of about -0.30 for the northern region and -0.40 for the southern region. The AMM, the equivalent of PMM in Atlantic region, and the AMO, which has been in its positive phase since 1995 (Wang et al., 2011), seem to affect coastal upwelling by modifying SSTs around the northwestern (NW) African coastline. Nevertheless, also the NAO climate index correlates significantly with the Canary tracer time series in our analysis (0.10 and 0.14 for NCanCS and SCanCS, respectively). This relationship is likely due to the strength of the Azores semi-permanent high-pressure system, which modifies trade wind strengths, and so the wind fields across the NW African upwelling zone, especially in winter (Cropper et al., 2014). One interesting feature of this analysis is that Atlantic (Pacific) upwelling indices only significantly correlate with the Atlantic (Pacific) climate modes. Not even ENSO, typically proposed as a bridge between basins, seems to affect the Atlantic Ocean, suggesting the absence of teleconnetion between

	Pacific				
	Mode 1	Mode2		Mode 1	Mode2
VexpTOT	50%	21%		51%	27%
NBenCS	65%	10%	NCalCS	46%	31%
SBenCS	50%	12%	SCalCS	51%	26%
NCanCS	58%	31%	NHCS	55%	24%
SCanCS	46%	32%	SHCS	51%	28%

Table 4.3: Percentage of variance explained by each mode.

upwelling systems in the two basins. Moreover, the southern and northern components of the upwelling systems correlate almost equally with climate modes. The only exception is the Benguela system, where AAO seems to affect both sub-regions and ATL-3 only the northern one.

4.4.2 Shared climate variability across EBUS

In addition to the link between each EBUS and climate modes, we study the shared upwelling variability across systems. To address this task, we performed an EOF analysis of UI across all the EBUS. As expected from the previous analysis, we find that most of the Atlantic and Pacific variability are largely independent. In fact, the loadings of the first and the second principal components (PC1 and PC2), namely the correlation between UI and PCs (Figure ??b), and their spatial structure in SST anomaly (Figure ??a), which are inferred by correlating PCs with NOAA SSTa, are representative of Atlantic Systems and Pacific Systems respectively. Therefore, we examine the variability in the two basins separately.

In the Pacific basin, as the left panels of Figure ?? show, the dominant shared mode, not surprisingly, is ENSO and its low-frequency modulation (TPDV). In fact, PC1-P, which explains 50% of the California and Peru total variance (Table 4.3, Pacific column), correlates approximately 0.65 and -0.6 with MEI and TPDV indices.

In the Atlantic, we find significant trend in upwelling that emerges as dominant mode (right panels of Figure ??), explaining approximately 60% and 50% of Benguela and Canary variance, respectively (Table 4.3). The spatial structure of the trends in the SSTa exhibit different signs and amplitude with a positive/strong trend in the Canary Systems and a negative/weak trend in the Benguela Systems. The warm (cold) trend reflects a negative (positive) trend in the concentration of the tracer. As previously discussed, the trend is driven by wind changes, even though part of Canary tendency appears to be related to RFI/stratification. Nevertheless, correlation analysis with climate modes reveals that it is also related to AMO. In fact the correlation between AMO and PC1-A is of about 0.50.

AMO modulates the inter-hemispheric meridional gradient of SST and, in turn, of SLP over the Atlantic ocean (Enfield et al., 2001). Thus, during its positive phase, atmospheric pressure difference at surface between North and South Atlantic lead to south-westerly (south-easterly) wind anomaly in NH (SH) (Wang et al. (2012), Gill (1980), Green et al. (2017)), which tends to weaken trades wind along Canary Systems and to enhanced them along Benguela Systems coast (e.g. same mechanism that shifts the ITCZ northward during warm AMO phase). Moreover, warm SST over north Atlantic enhances stratification and, thus, disfavours upwelling in Canary Systems.

In the second mode of Pacific basin (Figure??), we find a pattern in the SSTa with opposite signs in the northern and the southern hemispheres, suggesting a coherent response of the California and the Humboldt upwelling systems. This dipole is also evident in the large scale SLP structure obtained as correlation between NCEP SLPa and the Pacific PC2 (Figure ??a, right panel). However, a closer inspection reveals that the global footprint of the PC2-P does not reflect a real Pacific-basin mode. As a matter of fact, two indices (e.g. NPC2-P, SPC2-P), obtained by projecting the correction pattern off California System (Figure ??a, red square) and Peru System (Figure ??a, blue square) into the SSTa, do not show this dipole when correlated with NOAA SSTa (Figure ??b) and NCEP SLPa (Figure ??c). By consequence, NPC2-P index is characteristic of the second mode of Northern Pacific variability while SPC2-P represents the second mode of Southern Pacific variability. Correlation analysis, as suggested by the spatial pattern in Figure??b (left panel), reveals that NPC2-P is connected to Pacific Meridional Mode (PMM, see Figure?? for spatial pattern) with a correlation of -0.6 (Figure ??d). Controversially, the remaining variability of Humboldt System, SPC2-P, as suggested by the spatial pattern in Figure ??c (right panel), is connected to South Pacific Antarctic Oscillation (SAAO-P) with a correlation of 0.74 (Figure ??e). To obtain SAAO-P, we applied the same method used to calculate the SPC2-P. Namely, we project AAO correction pattern over the South Pacific domain, defined by the blue square, into NOAA SSTa (see Figure??). Moving to Atlantic basin, the 2nd mode of variability is dominated by Canary, explaining about 30% of Canary Systems variance and 15% of Benguela systems variance (see Table 4.3). PC2 is characterized by a large-scale SST structure resembling the AMM signature in the North Atlantic (Figure ??a and Figure?? for AMM spatial pattern) instead, in Southern Atlantic the SLPa pattern may evoke a -AAO like pattern (compare Figure ??c right panel and Figure ??). By consequence, we applied to the Atlantic second mode of variability the same reasoning and indexing used for Pacific basin. We calculate NPC2-A, SPC2-A as the projections the correction pattern off Canary Systems (Figure ??a, red square) and Benguela Systems (Figure ??a, blue square) into the NOAA SSTa respectively and, we obtained the South Atlantic Antarctic Oscillation (SAAO-A) projecting AAO correction pattern over the South Atlantic domain, defined by the red square, into NOAA SSTa (see Figure??). Correlation analysis of NPC2-A with AMM reveals high correlation of 0.79 (Figure ??d) while the remaining variability of Benguela (SPC2-A), is connected SAAO-A with a correlation of -0.79 (Figure ??e). The reason why AMM and PMM indices are not evaluated in the restricted domains is because of they are basin-scale climate modes (AMM for the Atlantic and PMM for the Pacific), while AAO by construction represent either South Atlantic and South Pacific variability. In summary, Pacific Systems share variability via ENSO while Atlantic results pooled by the trends, which are correlated to AMO. The remaining variability, instead, reveals sub-basin variability, influenced by Meridional Modes in the Northern Hemisphere and by AAO in the Southern Hemisphere. Therefore, circumpolar westerly flow influences upwelling favourable winds in Southern Atlantic and Pacific (Jones and Widmann, 2004), while stochastic wind and SST patterns linked to AMM and PMM tends to affect North Atlantic and Pacific upwelling.

4.5 Discussion and conclusions

In this study, we use a global eddy-permitting configuration of the NEMO ocean model forced by a new atmospheric forcing product (with a spatial resolution of 25 km) obtained through a statistical downscaling. The aim is to simulate the dynamics of EBUS and analyze the trends and the interannual-to-decadal variability within and across these areas from 1958 to 2015. In particular, to better reproduce winds along EBUS, we derived downscaled winds from the JRA55dov.1.1 reanalysis (Tsujino et al., 2018), taking advantage of the availability of QuikSCAT-based gridded product from IFREMER. We have shown that our numerical simulation (TRD55) captures the large-scale dynamics over the whole ocean (Figure ??) and over the upwelling areas, in particular over the Pacific systems (Figure ??). To explore the low-frequency upwelling variability, we presented a method to track nutrient-rich coastal waters, following Combes et al. (2013). In fact, the vertical transport of coastal water masses has been explored using passive tracers, continuously released in the subsurface ocean (depth range 150-300m) in each domain. The surface concentration of the tracers is used as a upwelling index (e.g. UI, UI_{slw} indices). The choice of these tracers allows us to represent the upwelling of nutrients usually located at sub-surface, that are at the base of the high productivity in EBUS. We first analyzed the upwelling seasonal cycle and its low-frequency modulation. The simulation is found to reproduce well the seasonal cycle of upwelling intensity over all EBUS areas when compared to seasonal cycle of AVISO sea surface height (Figures?? -?? panels e). Furthermore, a comparison of seasonal cycles of upwelling and meridional wind stress revealed that upwelling maxima generally occur when meridional winds are enhanced. This is consistent with the simple theories about the response of seasonal coastal upwelling to alongshore wind stresses (Bakun, 1990). Nevertheless, NHCS upwelling maxima presented a shift of one season

with respect to the meridional wind stress, while NBenCS does not show any enhanced upwelling during spring when upwelling-favourable winds are strong. Our understanding is that in the former the shift can be accounted for the enhanced eddy activity and the wind stress curl during boreal fall (Figure ??), while the latter is due to the intrusion of warm and salty water in boreal spring that intensifies stratification and weakens the upwelling (Figure ??), as shown in Shannon et al. (1987) and Rouault et al. (2007). Even though upwelling is driven by the meridional wind stress at seasonal scales, the upwelling interannual variability appears to follow different drivers, at least in the Canary and California systems. The linear regression analysis shows that, while the low-frequency variations of upwelling are primary driven by meridional wind stress in Benguela and SHCS, they are driven by the water column stratification in the Canary and California systems (Figure ??). In the NHCS, instead, wind stress curl and stratification are the major drivers, coherent with the finding on the climatological seasonal cycle. Our approach suggests that long-term upwelling variation cannot just be assessed and predicted by considering changes in wind stress intensity, as it is usually estimated, but the role of the ocean stratification needs to be considered, as Di Lorenzo et al. (2005) and Jacox et al. (2015) already discussed for the California systems. Furthermore, even though SST index is highly negative correlated with our upwelling index, it shows some discrepancies especially in the Benguela systems. Our results on low-frequency modulation of upwelling outline that neither the meridional winds or the SST-based indices could be used to properly identify upwelling variability in all the EBUS, leading to its misinterpretation and misrepresentation. Therefore, even though the EBUS seem to call for a common response, driven by the wind stress structures (Small et al. (2015) and Chapter 3), in a long-term variability upwelling is significantly different in each EBUS, discouraging a common theory on their future projections (EBUS Prospectus). In this matter, another important result of this study is indeed the partially disagreement between our analysis and the hypothesis of Bakun (1990). He postuled a long-term intensification of coastal of upwelling due to enhanced meridional wind stress, trigged by greenhouse gasses. The regions where Bakun hypothesis holds are Northern and Southern Benguela. There, we found positive significant trends driven by the enhanced meridional wind stress. By contrast, the Canary systems present significant negative trends and, as discussed above, not all the systems are primarily driven by the wind stress. In fact, in California and Peru systems neither the upwelling or its drivers (the upwelling-favourable winds and the stratification) show significant trends, in agreement to Combes et al. (2015) and Combes et al. (2013). Furthermore, trends coherency between northern and southern domains of Benguela and Canary systems do not support either the theory on the poleward displacement of high pressure-systems that should favorite upwelling poleward (Rykaczewski et al., 2015a). For the NCanCS, these results are in line with previous studies, such as Pardo et al. (2011), Pérez et al. (2010) and Gómez-Gesteira et al. (2011), where negative trends are detected both in SST index and in wind stress, and the Bakun hypothesis is not supported. More complicated is the interpretation of Benguela and SCanCS trends, which published results are conflicting. Depending on the analysed period as well as the data set used no trend (Dai et al., 2009), positive trends (Narayan et al. (2010); Santos et al. (2012), (Cropper et al., 2014)), and a negative trend (Narayan et al. (2010), Pardo et al. (2011), Gómez-Gesteira et al. (2008)) for upwelling in Benguela and Canary systems have been detected. Once again, the discrepancies found between our results and the previous literature highlights the importance of variable used as upwelling indicator, which, in light of the previous analysis, has to be identify in the relation to the major driver of each domain or be based on a composite of them. We also tried to address the influence of the large-scale climate variability on long-term upwelling. In fact, the variability associated with climate modes could be of importance to predict future perturbations at interannual to decadal time scales. Our correlation analysis showed that the Atlantic (Pacific) upwelling indices only significantly correlates with the Atlantic (Pacific) climate modes. In particular, the findings for the Pacific systems are in line with the published works. As previously detected in many studies, ENSO is the leading mode of variability of the Humboldt/Peru Systems (Cambon et al. (2013b), Combes et al. (2015), Renault et al. (2009)), while oscillations like PDO, NPGO and PMM are linked to the California systems variability (Di Lorenzo et al. (2008), Combes et al. (2013), Jacox et al. (2014), Macias et al. (2012)). In the Atlantic basin, Narayan et al. (2010), Pardo et al. (2011) showed Canary upwelling variability in associated with AMO and Cropper et al. (2014) also found influence induced by NAO. These connections are supported by our results even if the significant correlations with NAO are quite low. This lack of correlation is likely due to the fact that, in contrast to our work, Cropper et al. (2014) evaluated the link just during winter season (DJF). Instead, our findings for Benguela Systems differ from literature. Hagen et al. (2001) mentioned a possible influence of the Quasi-Biennial Oscillation (QBO) and Antarctic Oscillation (AAO), and according to some authors (e.g. Dufois and Rouault (2012)), ENSO signal could be of great importance. Our analysis rather has shown that the AAO climate mode influences both upwelling sub-regions, while ATL-3 could at most influence NBenCS. It is worth noting that we did not find any link with ENSO neither for Benguela or for Canary systems, even though some authors (e.g. Huang et al. (2007b)) suggest that ENSO, affecting the global tropical belt, also impacts the Atlantic upwelling systems. Finally, we presented a first attempt to understand to which extent the low-frequency variability of upwelling is shared across EBUS using an EOF analysis on the upwelling indices. We found that most of the variability of the Atlantic and the Pacific are largely independent, and so we treated them separately. The Pacific domains share dominance of ENSO variability whereas AMO is dominant in the Atlantic. The second modes of variability outlined the sub-basin scale variability. Surprisingly, we can argue that in

some extent Northern Hemisphere domains are controlled by meridional modes through the modulation of the wind and SST patterns while the Southern Hemisphere are influenced by Antarctica in particular by AAO, which regulate the strength of the circumpolar westerly flow and tends to influence equatorward favorable winds (Jones and Widmann, 2004). In summary, the drivers of low frequency variability of the EBUS, as simulated in a global high-resolution ocean simulation (TRD55), driven by a prescribed atmosphere in the last 6 decades, have been described in this paper. The major results are summarized as follows:

- 1. The low frequency variability of upwelling seasonal cycle regulates the interannual variability of the upwelling. Interestingly, EBUS domains differ in the low-frequency drivers. These results highlight the uniqueness of each EBUS and discourage the use of wind stress and SST-derived indices to study variability and the speculation about their common future projections.
- 2. Another important result is the partially disagreement between our analysis and the hypothesis of Bakun (1990). We found positive trend in upwelling intensity and in winds only over Benguela Systems. Canary systems show trends but they are negative and associated to enhanced stratification. In California and Humboldt/Peru systems neither the upwelling nor its drivers, the upwelling-favourable winds and the stratification show significant trends.
- 3. The estimated influence of the large-scale climate modes on EBUS results is reproduced only at basin-scale. Humboldt/Peru Systems are affect by ENSO, California by PDO and NPGO, Canary by AMO and Benguela by AAO. No teleconnection between basins is found. Not even ENSO, usually suggested as a bridge, seems to affect Atlantic Ocean, suggesting no teleconnection between upwelling systems in different basins.
- 4. For the first time, taking advantage of a global model, variability shared across EBUS has been evaluated. Any shared variability is found across all the EBUS. Pacific Systems shared variability via ENSO while Atlantic via AMO. The reminder variability of both basins, instead, surprisingly reveals sub-basin variability, influenced by Meridional Modes in the Northern Hemisphere and by AAO in the Southern Hemisphere.

The question of whether the variability observed here are indicative of interannual to multidecadal upwelling fluctuations is clouded both by the length of the time series, by the variable used to evaluate upwelling and by the use of a forced ocean-sea ice simulation. Extension of the current analysis to longer integration time of the numerical experiment, eventually employing a coupled model and with the same passive tracers' approach will

help to clarify these issues, to compare results obtained with the same approach and to verify better unexpected teleconnections between upwelling systems.

Chapter 5

Summary and Conclusions

In the scientific community, many aspects of EBUS dynamics and their variability are not fully understood. In particular, EBUS are still poorly represented in ocean and coupled models, and their future changes at interannual-to-decadal time scale under a changing climate still uncertain. In light of the unresolved scientific questions and the importance of EBUS on socio-economical activities, this thesis aims, for the first time in a global eddy-permitting ocean modelling framework, (1) to understand the impact of different wind structures on the upwelling dynamics and SST, and (2) to detect and compare low-frequency variability and changes in the EBUS. For these purposes, we performed three long-term hindcasts of the global ocean forced by three different atmospheric forcing. Namely, ERAInterim, the recent JRA55-do-v1.1 and a new atmospheric forcing product that we constructed through a statistical downscaling of the lower resolution JRA55 wind, merged with the high-resolution QuikSCAT observed winds. We used observation datasets (e.g. QuikSCAT, AVISO) and observational-based reanalyses (e.g. NCEP/NCAR, NOAA) for model validation. To facilitate the reading, ERAINT and JRA55 identify the atmospheric reanalyses, while ERAEXP and JRAEXP and TRD55 the three numerical simulations forced by ERAINT, JRA55 and the new downscaled product. In this chapter, the main results of this thesis are summarised giving answers to the research questions raised in the Introduction.

Is the observed variability of wind forcing in EBUS correctly represented in the atmospheric reanalyses? Is the observed variability of the ocean dynamical response in EBUS represented in the eddy-permitting ocean simulations?

We addressed these questions in Chapter 2, where we analyzed and validated the temporal varibility of the wind stress and wind stress curl represented in the atmospheric reanalyses (JRA55 and ERAINT) compared with the QuikSCAT measurements, and the variability of surface oceanic variables (Sea Surface Height and Sea Surface Temperature) simulated by the numerical simulations (JRAEXP and ERAEXP) against AVISO data and

NOAA SST. We found that the wind forcing mainly varies on seasonal scales, and the wind forcing within EBUS is latitude-dependent. Low latitudes experience mostly year-round upwelling-favourable wind (although still with a seasonal modulation), while higher latitudes are characterized by upwelling-favourable winds typically during the boreal (austral) spring and summer in the NH (SH) systems. Both the atmospheric reanalyses represent well the QuickSCAT observed variability at large scale, but show differences among them and deficiencies with respect to the observed winds in the coastal regions. In particular, maxima of the wind appear always too far from the coast, and the wind stress curl is too strong. By investigating the modeled ocean variability forced by the two atmospheric reanalyses, our results show that SST and SSH are also well represented in the numerical simulations. The principal feature that emerges from the analysis of ocean variability is that the character of the four EBUS is, to a great extent, dependent on basin-scale features: Pacific upwelling, especially the Peru system, is dominated by interannual variability (e.g. El Niño dynamics), the Benguela system by eddy-induced variability (intraseasonal variability) due to lateral remote advection from Indian Ocean; while, in the Atlantic, the Canary system is mainly dominated by seasonal variability, likely due to a large seasonal cycle of the solar radiation and SST. On the other hand, in all EBUS, SST variability results highly seasonal offshore and intraseasonal near the coast, influenced by upwelling events.

How does the currents system in EBUS change under different structures of the winds? Are the different EBUS responding in the same way to different wind forcing?

This questions are addressed in Chapter 3, where we compare the ocean response of JRAEXP and ERAEXP simulations. We argued that, in all the domains, stronger WSC associated with weak coastal wind, characteristic of ERAINT reanalysis, promote stronger offshore Ekman pumping and weak coastal veritcal velocity, while weak WSC associated with strong coastal wind, characteristic of JRA55, generate weak Ekman Pumping and localized intense coastal upwelling. In terms of meridional currents, weak WSC and strong TauY at coast promote alongshore equatorward upper-layer currents and a deep under-current, while strong WSC and weak TauY promote WSC-driven currents and thus flow upwind. These meridional current discrepancies in the two experiments, as expected, are mirrored on the averaged meridional transport estimates over EBUS, highlighting interesting asymmetry on the transport structure in the water column. JRAEXP solution is characterized by strong and deep transport in the direction of the wind (equatorward, negative in NH and positive in SH hemisphere), while ERAEXP shows equatorward transport only at surface.

Are we improving SST biases in an eddy-permitting ocean model using high-resolution atmospheric reanalyses?

This question is motived by the well-known warm SST biases characteristic of both ocean and coupled models. The answer is presented in Chapter 3, comparing SST fields computed in JRAEXP and ERAEXP experiments. The SST warm bias evident in the ocean driven by ERAINT is generally damped in JRA55EXP, especially along the coast. We attributed this improvement to the enhanced coastal upwelling and equatorward advection reproduced in the JRAEXP simulation, which is driven by weak WSC associated to a strong coastal wind. We also underlined that, since we used two different reanalyses, variations in heat fluxes over the air-sea interface play a role in setting these SST differences. Nevertheless, a linear regression model between SST differences (JRAEXP-ERAEXP) as predictand and differences in wind and in downward incoming heat flux as predictors, shows that the contribution of the wind on SST differences at interannual and intraseasonal time scales is always greater than the contribution of incoming heat fluxes, explaining at least 40% of its variation. The only exception is the Canary System where the heat flux contribution is the largest at intraseasonal scale.

Which are the drivers of low-frequency variability on EBUS? Are there any trends?

This question is answered in Chapter 4, where the results of the TRD55 simulation are analyzed. Motivated by the importance of the wind at coast over EBUS, we forced TRD55 by a new wind forcing (25 km of horizontal resolution over EBUS) that we obtained through a statistical downscaling. This method allowed us to potentially better represent the dynamics of upwelling and to released passive tracers in the ocean subsurface (150m-300m) from the coast to 50 km offshore in each EBUS, aiming to represent and follow the coastal subsurface waters, and to identify a proxy for coastal upwelling strength. Even if, at seasonal scale, upwelling is driven by the meridional wind stress, its interannual variability appears to follow different drivers. Our linear regression analysis shows that the low-frequency variations of the upwelling are primarily driven by meridional wind stress in Benguela and Peru regions, and by stratification in Canary and California systems. Regarding the trends, we found positive significant trends driven by the enhanced meridional wind stress. By contrast, the Canary systems present significant negative trends and, as discussed above, not all the systems are primarily driven by the wind stress. In fact, in California and Peru systems neither the upwelling or its drivers (the upwelling-favourable winds and the stratification) show significant trends, in agreement to Combes et al. (2015) and Combes et al. (2013). These results, except for Benguela, are in contrast to the wellknown hypothesis proposed by Bakun (1990), who stated that the land would heat up more rapidly than the ocean with increasing greenhouse gas concentrations, resulting in

an intensification of the air pressure contrast (high over the ocean and low over the land), and so leading to stronger trade winds over the EBUS.

Is there any shared decadal variability between EBUS? Is that variability driven by climate modes?

We addressed these questions in Chapter 4. For the first time in a study about EBUS, we tried to understand to which extent the low-frequency variability of upwelling is shared across EBUS using an EOF analysis on upwelling indices. We found that most of the variability in the Atlantic and the Pacific are largely independent, and so we treated them separately. The Pacific domains are dominated by ENSO variability, whereas AMO is the first dominant mode with influence on the upwelling systems in the Atlantic. The second modes outlined the sub-basin scale variability. Surprisingly, we can argue that, to some extent, the Northern Hemisphere domains are controlled by Meridional Modes (PMM and AMM) through the modulation of wind and SST patterns, while the Southern Hemisphere domains are influenced by Antarctica atmospheric variability, in particular by the AAO, which is affected by the strength of the circumpolar westerly flow, and can influence equatorward favorable winds.

In summary, this thesis provides insight on some of the unresolved scientific questions about the EBUS dynamics and variability. As regard to the model representation of EBUS, the global ocean eddy-permitting simulations forced by high-resolved biased-corrected atmospheric forcing (e.g. ERAINT and JRA55) suggest a coherent ocean circulation response over EBUS induced by the wind, and they helped to clarify the role of the wind on the warm sea surface temperature bias. The four wind-driven EBUS appear to call for a common climatological response of the regional oceanic circulation: coastal upwelling and Ekman pumping are locally forced by differences in alongshore wind stress and wind stress curl, respectively; equatorward currents are intensified under enhanced wind stress condition, while poleward undercurrents respond to WSC changes; SST differences are mostly related to a stronger nearshore wind stress rather than incoming heat fluxes due to enhanced vertical velocities and along-shore equatorward currents downwind. Nevertheless, examining the long-term variability, the upwelling presents significant differences in each EBUS. This thesis results indicate that the low-frequency upwelling variability in the EBUS, as detected using passive tracers, is induced by different low-frequency drivers, presents contrasting long-term trends, and does not share any interannual-to-decadal variability across basins. Common theory on their future projections, such as Bakun hypothesis, has therefore to be revised in light of the different drivers of each system. Extension of the current analysis to longer time scales with enhanced wind forcing resolution and with higher resolution forced and coupled models in a global framework are needed to support these results, to clarify further the role of the wind forcing and of the heat fluxes on these areas and to better study the long-term variability of EBUS.

Appendix A

Downscaling Method

The extreme sensitivity of EBUS to the specific structure of the wind, as presented in Chapter 3, pushed us to develop a new high-resolution dataset of wind that merges reanalysis product with scatterometer observations. For this purpose, we compute a regional statistical downscaling of the JRA55 wind over EBUS using QuickSCAT wind retrivials. As already mentioned in Chapter 4, we follow the method by Goubanova et al. (2011). The main idea of the statistical downscaling consists in building a statistical relationship between local/regional variables (predictand) and large-scale climate characteristics (predictors) for the period when predictand, usually observations, is available. This relationship is then applied to predictors to the past or to the future. In this way, it is possible to correct the predictor fields even when the observations are not available. The predictand is the 10m near-surface daily wind measured by QuikSCAT scatterometer (gridded product from IFREMER, with a 0.25° spatial resolution in latitude and longitude) over the period 2000-2008. This product is assumed to offer the best quality long-term daily time series. The large-scale predictors are the sea level pressure and near-surface wind fields from the JRA55 reanalysis, in the same time-window. The statistical relations between predictand and predictors are then used to downscale JRA55 surface winds for the period 1958-2015 obtaining a new high-resolution dataset (same resolution of predict and, 25 km), corrected by observations.

An appropriate selection of the predictor variables based on physical consideration is one of the most important steps in the development of a statistical downscaling algorithm. Naturally, predictors for the surface wind need to represent the large scale atmospheric circulation. Hence, for our downscaling scheme the large-scale, meridional and zonal wind at 10 m and sea level pressure are chosen as predictors informative about the larger-scale atmospheric dynamics. To identify the optimal geographic location of the predictor variables, the standardized SLP from JRA55 reanalysis are regressed onto the standardized QuikSCAT winds at the main coastal jet zones, in all the domains: at 17.75°S-13.2°E, 27.25°S-15.5°E, 33.75°S-18.25°E for the BenCS, at 39.75°N-10.5°W, 31.5°N-10°W and 24.5°N-14.25°W for

the CanCS, at 42.5°N-122.25°W and 31.5°N-115.25°W for the CalCS and at 9°S-76.5°W, 15°S-75.5°W, 38°S-73.5°W for the HCS. The results are displayed in Figures ??-??-? ??. The obtained pattern indicates that the region actively influencing the variability all the upwelling domains corresponds to the mean position of the anticyclones, in particular South Atlantic Anticyclone near BenCS, the North Atlantic Subtropical anticyclone (or Azores High) off CanCS, the North Pacific High near CalCS, and South Pacific Anticyclone off HCS. Therefore, the downscaling domain for the predictor variables is chosen in order to include the zone with the maximum correlation between coastal jets and SLP (red squares in Figures ??-??-??). The predictand areas are represented by blue squares. Once defined the predictor/predict and areas, the statistical relationship is built in the empirical orthogonal functions (EOF) space. The EOFs are computed from the anomalies relative to the mean seasonal cycle for the period 2000-2008. For the predictand, EOFs are obtained based on the covariance matrix containing QuikSCAT zonal and meridional wind anomalies. The predictor EOFs are computed from the correlation matrix containing SLP, zonal and meridional wind anomalies from JRA55 reanalysis. The predictor-predictand relationship is built for the principal components corresponding to the retained EOFs and has the form:

$$PCQ_i = \sum_{j=1}^{150} \alpha_{ij} PCJ_j + \epsilon, i = 1:100$$
 (A.1)

where PCQ_i are the i^{th} QuikSCAT PC time series, ij are the regression coefficients, PCJ_j are the PCs of the JRA55 time series and is the regression error. See later for the choice of the number of EOFs retained. Once obtained the regression coefficients, to downscale JRA55 over EBUS during the period where data are not available, we first compute the anomalies of the corresponding JRA55 predictor variables (X). Then, these anomalies are projected onto the predictors EOF space. By applying the regression coefficients to these projections, the time series can be obtained over the high-resolution domain:

$$PCX_j = \sum_{j=1}^{150} \alpha_{ij}(XEOFJ_i), i = 1:100$$
(A.2)

where X is the anomalies of JRA55 predictors, $EOFJ_j$ is the j^{th} JRA55 eigenvector. It is worth mentioning that the relation holds for anomalies relative to the present climate seasonal cycle, therefore JRA55 anomalies are obtained relative to the present climate seasonal cycle. Low-frequency modulation and trends are in this way preserved in the anomalies. The downscaled fields are finally reconstructed following:

$$Y_{DS} = PCX * EOFQ \tag{A.3}$$

where PCX are the time series obtained in Equation A.2, EOFQ are the QuikSCAT eigenvector and Y_{DS} are the downscaled anomalies of meridional and zonal wind relative

to the present climate seasonal cycle. The total wind field can be obtained by adding the seasonal cycle as derived previously from QuikSCAT to the downscaled anomalies. The number of EOFs retained to build the relationship is based on tests effectuated on downscaled wind over a specified area off Benguela System (33°S - 34°S, green square Figure ??a) for the 2001. As Figure ?? shows, we studied the correlation between the downscaled product (Y_{DS}) and QuikSCAT (considered our reference) as a function of the number of retained EOFs in the downscaling method (Equation A.1). First, we fixed QuikSCAT EOFs number changing JRA55 EOFs (blue line, Qfix), and then we fixed JRA55 EOFs number changing QuickSCAT EOFs one (black line, Jfix). The bold number in each panel represents the number of EOFs fixed for QuikSCAT when blue line is calculated, and for JRA55 when the black line is calculated. Looking at Figure ??, changes in QuikSCAT EOFs (black line, Jfix) do not lead to significant difference once the number of JRA55 EOFs is assigned. Nevertheless, to obtain a good result we need at least 100 of JRA55 EOFs, indeed correlation coefficient changes from 0.5 to 0.7 values from panels a (10 EOFs) and b (100 EOFs). For these reasons for the study purpose we retained 150 EOFs for JRA55 and 100 EOFs for QUIKSCAT. We decided for 100 QuikSCAT because it worth noting that there is a little increase of correlation coefficient considering EOFs in Figure ?? when JRA55 is fixed to 150 (blue cycle) and because the choice of less EOFs does not significatively improve the computational time.

In order to obtain the global fields to drive the global ocean circulation in our NEMO simulation, we merged the new regional high resolution downscaled product into the original JRA55 product (Figure ??). Due to the difference in the horizontal resolution, 25 km for Y_{DS} and 55 km for JRA55, we interpolated both on the tripolar ORCA grid at $1/4^{\circ}$. Then, we added a diurnal cycle extracted from JRA55 to Y_{DS} in order to obtain the same temporal resolution (3h) and merged the two products considering a buffer zone (Figure ?? panels c,d) of 10 grid points to avoid discontinuity between the two products. In the buffer zone, the new forcing is a weighted average of the two products depending on the distance from the downscaled domain:

$$Y_{BU} = (1 - \beta)JRA55 + \beta Y_{DS} \tag{A.4}$$

where β is a parameter that increase from 0 to 1 towards the downscaled domains of 1/10 each grid point. In summary, as Figure ?? shows, JRA55 wind interpolated on NEMO grid (Figure ??a) is multiplicated by $(1-\beta)$ (Figure ??c), Y_{DS} (Figure ??b) is multiplied by β (Figure ??d), and then they are added to each other to create the global new wind forcing (Figure ??e). Examples of the new forcing are reported in Figures ?? and ??. Y_{DS} forcing (Figure ?? panels c) resemble much better the spatial variability of wind (top panels) and wind curl (bottom panels) of QuikSCAT rather than JRA55 fields (panels a). Moreover, looking at wind curl times series (Figure ??), obtained as a mean the red and blue squares

in Figure ??, also the temporal variability is well represented by the new dataset.

Bibliography

- Albert, A., V. Echevin, M. Lévy, and O. Aumont, 2010: Impact of nearshore wind stress curl on coastal circulation and primary productivity in the peru upwelling system. *Journal of Geophysical Research: Oceans*, 115 (C12).
- Amante, C., and B. W. Eakins, 2009: Etopo1 global relief model converted to panmap layer format. NOAA-National Geophysical Data Center, doi, 10.
- Arístegui, J., and Coauthors, 2009: Sub-regional ecosystem variability in the canary current upwelling. *Progress in Oceanography*, **83** (1-4), 33–48.
- Bakun, A., 1975: Daily and weekly upwelling indices, west coast of north america. *NOAA Tech*, **16**.
- Bakun, A., 1990: Global climate change and intensification of coastal ocean upwelling. *Science*, **247** (4939), 198–201.
- Bakun, A., D. B. Field, A. Redondo-Rodriguez, and S. J. Weeks, 2010: Greenhouse gas, upwelling-favorable winds, and the future of coastal ocean upwelling ecosystems. *Global Change Biology*, **16** (4), 1213–1228.
- Bakun, A., and C. S. Nelson, 1991: The seasonal cycle of wind-stress curl in subtropical eastern boundary current regions. *Journal of Physical Oceanography*, **21** (12), 1815–1834.
- Barnston, A. G., and R. E. Livezey, 1987: Classification, seasonality and persistence of low-frequency atmospheric circulation patterns. *Monthly weather review*, **115** (6), 1083–1126.
- Belkin, I. M., 2009: Rapid warming of large marine ecosystems. *Progress in Oceanography*, **81** (1-4), 207–213.
- Bentamy, A., D. Croize-Fillon, and C. Perigaud, 2008: Characterization of ascat measurements based on buoy and quikscat wind vector observations. *Ocean Science*, 4 (4), 265–274.

- Bentamy, A., and D. C. Fillon, 2012: Gridded surface wind fields from metop/ascat measurements. *International journal of remote sensing*, **33** (6), 1729–1754.
- Bernard, B., and Coauthors, 2006: Impact of partial steps and momentum advection schemes in a global ocean circulation model at eddy-permitting resolution. *Ocean dynamics*, **56** (5-6), 543–567.
- Blamey, L. K., and Coauthors, 2015: Ecosystem change in the southern benguela and the underlying processes. *Journal of Marine Systems*, **144**, 9–29.
- Cambon, G., and Coauthors, 2013a: Assessing the impact of downscaled winds on a regional ocean model simulation of the humboldt system. *Ocean Modelling*, **65**, 11–24.
- Cambon, G., and Coauthors, 2013b: Assessing the impact of downscaled winds on a regional ocean model simulation of the humboldt system. *Ocean Modelling*, **65**, 11–24.
- Capet, X. J., P. Marchesiello, and J. C. McWilliams, 2004: Upwelling response to coastal wind profiles. *Geophysical Research Letters*, **31**, 13.
- Cessi, P., and C. L. Wolfe, 2009: Eddy-driven buoyancy gradients on eastern boundaries and their role in the thermocline. *Journal of Physical Oceanography*, **39** (7), 1595–1614.
- Chavez, F., and Coauthors, 2002: Biological and chemical consequences of the 1997–1998 el niño in central california waters. *Progress in Oceanography*, **54** (1-4), 205–232.
- Chavez, F. P., and M. Messié, 2009: A comparison of eastern boundary upwelling ecosystems. *Progress in Oceanography*, **83** (1-4), 80–96.
- Chen, Z., and Coauthors, 2012: A study of benguela upwelling system using different upwelling indices derived from remotely sensed data. *Continental shelf research*, **45**, 27–33.
- Chhak, K., and E. Di Lorenzo, 2007: Decadal variations in the california current upwelling cells. *Geophysical Research Letters*, **34** (14).
- Chiang, J. C., and D. J. Vimont, 2004: Analogous pacific and atlantic meridional modes of tropical atmosphere—ocean variability. *Journal of Climate*, **17** (21), 4143–4158.
- Choi, J., S.-I. An, S.-W. Yeh, and J.-Y. Yu, 2013: Enso-like and enso-induced tropical pacific decadal variability in cgcms. *Journal of Climate*, **26** (5), 1485–1501.
- Colas, F., J. C. McWilliams, X. Capet, and J. Kurian, 2012: Heat balance and eddies in the peru-chile current system. *Climate dynamics*, **39** (1-2), 509–529.

- Collins, W. D., and Coauthors, 2006: The community climate system model version 3 (ccsm3). *Journal of Climate*, **19 (11)**, 2122–2143.
- Combes, V., and Coauthors, 2013: Cross-shore transport variability in the california current: Ekman upwelling vs. eddy dynamics. *Progress in Oceanography*, **109**, 78–89.
- Combes, V., S. Hormazabal, and E. Di Lorenzo, 2015: Interannual variability of the subsurface eddy field in the southeast pacific. *Journal of Geophysical Research: Oceans*, **120** (7), 4907–4924.
- Cropper, T. E., E. Hanna, and G. R. Bigg, 2014: Spatial and temporal seasonal trends in coastal upwelling off northwest africa, 1981–2012. *Deep Sea Research Part I: Oceano-graphic Research Papers*, 86, 94–111.
- Curchitser, E., J. Small, K. Hedstrom, and W. Large, 2011: 3.7 up-and down-scaling effects of upwelling in the california current system. *Report of Working Group*, **20**.
- Dai, A., T. Qian, K. E. Trenberth, and J. D. Milliman, 2009: Changes in continental freshwater discharge from 1948 to 2004. *Journal of climate*, **22** (10), 2773–2792.
- Dai, A., and K. E. Trenberth, 2002: Estimates of freshwater discharge from continents: Latitudinal and seasonal variations. *Journal of hydrometeorology*, **3 (6)**, 660–687.
- Dee, D. P., and Coauthors, 2011: The era-interim reanalysis: Configuration and performance of the data assimilation system. *Quarterly Journal of the royal meteorological society*, **137** (656), 553–597.
- Demarcq, H., 2009: Trends in primary production, sea surface temperature and wind in upwelling systems (1998–2007). *Progress in Oceanography*, **83 (1-4)**, 376–385.
- Desbiolles, F., B. Blanke, and A. Bentamy, 2014: Short-term upwelling events at the western african coast related to synoptic atmospheric structures as derived from satellite observations. *Journal of Geophysical Research: Oceans*, **119** (1), 461–483.
- Dewitte, B., and Coauthors, 2011: Modes of covariability between sea surface temperature and wind stress intraseasonal anomalies along the coast of peru from satellite observations (2000–2008). *Journal of Geophysical Research: Oceans*, **116** (C4).
- Dewitte, B., and Coauthors, 2012: Change in el nino flavours over 1958–2008: Implications for the long-term trend of the upwelling off peru. Deep Sea Research Part II: Topical Studies in Oceanography, 77, 143–156.
- Di Lorenzo, E., A. J. Miller, N. Schneider, and J. C. McWilliams, 2005: The warming of the california current system: Dynamics and ecosystem implications. *Journal of Physical Oceanography*, **35** (3), 336–362.

- Di Lorenzo, E., and Coauthors, 2008: North pacific gyre oscillation links ocean climate and ecosystem change. *Geophysical Research Letters*, **35** (8).
- Dufois, F., and M. Rouault, 2012: Sea surface temperature in false bay (south africa): towards a better understanding of its seasonal and inter-annual variability. *Continental Shelf Research*, **43**, 24–35.
- Enfield, D. B., A. M. Mestas-Nuñez, and P. J. Trimble, 2001: The atlantic multidecadal oscillation and its relation to rainfall and river flows in the continental us. *Geophysical Research Letters*, **28** (10), 2077–2080.
- Fennel, W., T. Junker, M. Schmidt, and V. Mohrholz, 2012: Response of the benguela upwelling systems to spatial variations in the wind stress. *Continental Shelf Research*, 45, 65–77.
- Fennel, W., and H. U. Lass, 2007: On the impact of wind curls on coastal currents. *Journal of Marine Systems*, **68** (1-2), 128–142.
- Fichefet, T., and M. M. Maqueda, 1997: Sensitivity of a global sea ice model to the treatment of ice thermodynamics and dynamics. *Journal of Geophysical Research: Oceans*, 102, 12609–12646.
- García-Reyes, M., and J. Largier, 2010: Observations of increased wind-driven coastal upwelling off central california. *Journal of Geophysical Research: Oceans*, **115** (C4).
- García-Reyes, M., and J. Largier, 2012: Seasonality of coastal upwelling off central and northern california: New insights, including temporal and spatial variability. *Journal of Geophysical Research: Oceans*, **117** (C3).
- García-Reyes, M., and Coauthors, 2015: Under pressure: Climate change, upwelling, and eastern boundary upwelling ecosystems. Frontiers in Marine Science, 2, 109.
- Garreaud, R., and R. C. Muñoz, 2005: The low-level jet off the west coast of subtropical south america: Structure and variability. *Monthly Weather Review*, **133** (8), 2246–2261.
- Garreaud, R. D., and M. Falvey, 2009: The coastal winds off western subtropical south america in future climate scenarios. *International Journal of Climatology: A Journal of the Royal Meteorological Society*, **29** (4), 543–554.
- Gill, A., 1980: Some simple solutions for heat-induced tropical circulation. *Quarterly Journal of the Royal Meteorological Society*, **106** (449), 447–462.
- Gill, A. E., 2016: Atmosphere-ocean dynamics. Elsevier.

- Gómez-Gesteira, M., and Coauthors, 2008: Spatio-temporal upwelling trends along the canary upwelling system (1967–2006). Annals of the New York Academy of Sciences, 1146 (1), 320–337.
- Gómez-Gesteira, M., and Coauthors, 2011: The state of climate in nw iberia. *Climate Research*, **48** (2-3), 109–144.
- Gómez-Letona, M., A. G. Ramos, J. Coca, and J. Arístegui, 2017: Trends in primary production in the canary current upwelling system-a regional perspective comparing remote sensing models. *Frontiers in Marine Science*, 4, 370.
- Goubanova, K., and Coauthors, 2011: Statistical downscaling of sea-surface wind over the peru-chile upwelling region: diagnosing the impact of climate change from the ipsl-cm4 model. Climate Dynamics, 36 (7-8), 1365–1378.
- Green, B., J. Marshall, and A. Donohoe, 2017: Twentieth century correlations between extratropical sst variability and itcz shifts. *Geophysical Research Letters*, **44** (17), 9039–9047.
- Gutiérrez, D., and Coauthors, 2011: Coastal cooling and increased productivity in the main upwelling zone off peru since the mid-twentieth century. *Geophysical Research Letters*, 38 (7).
- Hagen, E., R. Feistel, J. J. Agenbag, and T. Ohde, 2001: Seasonal and interannual changes in intense benguela upwelling (1982–1999). Oceanologica Acta, 24 (6), 557–568.
- Hu, Z. Z., B. Huang, and K. Pegion, 2008: Low cloud errors over the southeastern atlantic in the neep cfs and their association with lower-tropospheric stability and air-sea interaction. *Journal of Geophysical Research: Atmospheres*, **113**.
- Huang, B., Z.-Z. Hu, and B. Jha, 2007a: Evolution of model systematic errors in the tropical atlantic basin from coupled climate hindcasts. *Climate dynamics*, **28** (7-8), 661–682.
- Huang, B., Z. Z. Hu, and B. Jha, 2007b: Evolution of model systematic errors in the tropical atlantic basin from coupled climate hindcasts. *Climate dynamics*, **28** (7-8), 661–682.
- Hutchings, L., and Coauthors, 1998: Multiple factors affecting south african anchovy recruitment in the spawning, transport and nursery areas. South African Journal of Marine Science, 19 (1), 211–225.
- Jacobs, S. S., H. H. Hellmer, and A. Jenkins, 1996: Antarctic ice sheet melting in the southeast pacific. *Geophysical Research Letters*, **23** (9), 957–960.

- Jacox, M., A. Moore, C. Edwards, and J. Fiechter, 2014: Spatially resolved upwelling in the california current system and its connections to climate variability. *Geophysical Research Letters*, **41** (9), 3189–3196.
- Jacox, M. G., S. J. Bograd, E. L. Hazen, and J. Fiechter, 2015: Sensitivity of the california current nutrient supply to wind, heat, and remote ocean forcing. *Geophysical Research Letters*, **42** (14), 5950–5957.
- Jones, J. M., and M. Widmann, 2004: Atmospheric science: Early peak in antarctic oscillation index. *Nature*, **432** (7015), 290.
- Jr, C., D. M., and J. A. Barth, 2009: Patterns and processes in the california current system. *Progress in Oceanography*, **83** (1-4), 49–64.
- Junker, T., M. Schmidt, and V. Mohrholz, 2015: The relation of wind stress curl and meridional transport in the benguela upwelling system. *Journal of Marine Systems*, **143**, 1–6.
- Kirkman, S., and Coauthors, 2016: Spatial characterisation of the benguela ecosystem for ecosystem-based management. *African Journal of Marine Science*, **38** (1), 7–22.
- Labitzke, K., and H. Van Loon, 1992: On the association between the qbo and the extratropical stratosphere. *Journal of atmospheric and terrestrial physics*, **54** (11-12), 1453–1463.
- Large, W. G., and G. Danabasoglu, 2006: Attribution and impacts of upper-ocean biases in ccsm3. *Journal of Climate*, **19** (**11**), 2325–2346.
- Large, W. G., and S. G. Yeager, 2004: the data sets and flux climatologies, Diurnal to decadal global forcing for ocean and sea-ice models.
- Lebassi, B., and Coauthors, 2009: Observed 1970–2005 cooling of summer daytime temperatures in coastal california. *Journal of Climate*, **22** (13), 3558–3573.
- Lehodey, P., and Coauthors, 2006: Climate variability, fish, and fisheries. *Journal of Climate*, **19** (20), 5009–5030.
- Lluch-Belda, D., and Coauthors, 1989: World-wide fluctuations of sardine and anchovy stocks: the regime problem. South African Journal of Marine Science, 8 (1), 195–205.
- LLUCH-BELDA, D., and Coauthors, 1992: Sardine and anchovy regime fluctuations of abundance in four regions of the world oceans: a workshop report. *Fisheries Oceanogra-phy*, **1** (4), 339–347.

- Macias, D., and Coauthors, 2012: Climatic control of upwelling variability along the western north-american coast. *PloS one*, **7** (1), e30 436.
- Madec, G., 2015: NEMO ocean engine.
- Madec, G., and M. Imbard, 1996: A global ocean mesh to overcome the north pole singularity. Climate Dynamics, 12 (6), 381–388.
- Mantua, N. J., and S. R. Hare, 2002: The pacific decadal oscillation. *Journal of oceanog-raphy*, **58** (1), 35–44.
- Marchesiello, P., and P. Estrade, 2010: Upwelling limitation by onshore geostrophic flow. Journal of Marine Research, 68 (1), 37–62.
- Marchesiello, P., J. C. McWilliams, and A. Shchepetkin, 2003a: Equilibrium structure and dynamics of the california current system. *Journal of physical Oceanography*, **33** (4), 753–783.
- Marchesiello, P., J. C. McWilliams, and A. Shchepetkin, 2003b: Equilibrium structure and dynamics of the california current system. *Journal of physical Oceanography*, **33** (4), 753–783.
- Marshall, J., and T. Radko, 2003: Residual-mean solutions for the antarctic circumpolar current and its associated overturning circulation. *Journal of Physical Oceanography*, **33 (11)**, 2341–2354.
- McCabe, R. M., B. M. Hickey, E. P. Dever, and P. MacCready, 2015: Seasonal cross-shelf flow structure, upwelling relaxation, and the alongshelf pressure gradient in the northern california current system. *Journal of Physical Oceanography*, **45** (1), 209–227.
- McCreary, J. P., and S. Y. Chao, 1985: Three-dimensional shelf circulation along an eastern ocean boundary. *Journal of marine research*, **43** (1), 13–36.
- Mendelssohn, R., and F. Schwing, 2002: Common and uncommon trends in sst and wind stress in the california and peru-chile current systems. *Progress in Oceanography*, **53** (2-4), 141–162.
- Messié, M., and Coauthors, 2009: Potential new production estimates in four eastern boundary upwelling ecosystems. *Progress in Oceanography*, **83 (1-4)**, 151–158.
- Minobe, S., and N. Mantua, 1999: Interdecadal modulation of interannual atmospheric and oceanic variability over the north pacific. *Progress in Oceanography*, **43** (2-4), 163–192.
- Narayan, N., A. Paul, S. Mulitza, and M. Schulz, 2010: Trends in coastal upwelling intensity during the late 20th century. *Ocean Science*, 6 (3), 815–823.

- Palter, J. B., 2015: The role of the gulf stream in european climate. *Annual review of marine science*, **7**, 113–137.
- Pardo, P. C., and Coauthors, 2011: Evolution of upwelling systems coupled to the long-term variability in sea surface temperature and ekman transport. *Climate Research*, **48 (2-3)**, 231–246.
- Parrish, R., F. B. Schwing, and R. Mendelssohn, 2000: Mid-latitude wind stress: the energy source for climatic shifts in the north pacific ocean. *Fish. Oceanogr.*, **9** (3), 224–238.
- Pauly, D., and V. Christensen, 1995: Primary production required to sustain global fisheries. *Nature*, **374** (6519), 255–257.
- Pelegrí, J., and Coauthors, 2005: Coupling between the open ocean and the coastal upwelling region off northwest africa: water recirculation and offshore pumping of organic matter. *Journal of Marine Systems*, **54** (1-4), 3–37.
- Pérez, F. F., and Coauthors, 2010: Plankton response to weakening of the iberian coastal upwelling. *Global Change Biology*, **16** (4), 1258–1267.
- Peterson, W. T., and F. B. Schwing, 2003: A new climate regime in northeast pacific ecosystems. *Geophysical research letters*, **30**, 17.
- Pickett, M. H., and J. D. Paduan, 2003: Ekman transport and pumping in the california current based on the us navy high-resolution atmospheric model (coamps). *Journal of Geophysical Research: Oceans*, **108**.
- Pietri, A., and Coauthors, 2014: Impact of a coastal-trapped wave on the near-coastal circulation of the peru upwelling system from glider data. *Journal of Geophysical Research:* Oceans, 119 (3), 2109–2120.
- Rebstock, G. A., 2003: Long-term change and stability in the california current system: lessons from calcofi and other long-term data sets. *Deep Sea Research Part II: Topical Studies in Oceanography*, **50** (14-16), 2583–2594.
- Renault, L., and Coauthors, 2009: Impact of atmospheric coastal jet off central chile on sea surface temperature from satellite observations (2000–2007). *Journal of Geophysical Research: Oceans*, **114** (C8).
- Renault, L., and Coauthors, 2012: Upwelling response to atmospheric coastal jets off central chile: A modeling study of the october 2000 event. *Journal of Geophysical Research: Oceans*, **117** (C2).

- Reynolds, R. W., and Coauthors, 2007: Daily high-resolution-blended analyses for sea surface temperature. *Journal of Climate*, **20** (22), 5473–5496.
- Richter, I., 2015a: Climate model biases in the eastern tropical oceans: Causes, impacts and ways forward. Wiley Interdisciplinary Reviews: Climate Change, 6 (3), 345–358.
- Richter, I., 2015b: Climate model biases in the eastern tropical oceans: Causes, impacts and ways forward. *Interdisciplinary Reviews: Climate Change*, 6(3, 345–358.
- Rodríguez-Fonseca, B., and Coauthors, 2009: Are atlantic niños enhancing pacific enso events in recent decades? *Geophysical Research Letters*, **36** (20).
- Roesler, C. S., 1987: Zooplankton variability in the california current. 1951–1982.
- Rouault, M., and Coauthors, 2007: Propagation and origin of warm anomalies in the angola benguela upwelling system in 2001. *Journal of Marine Systems*, **68** (3-4), 473–488.
- Rouault, M., B. Pohl, and P. Penven, 2010: Coastal oceanic climate change and variability from 1982 to 2009 around south africa. *African Journal of Marine Science*, **32** (2), 237–246.
- Rykaczewski, R. R., and Coauthors, 2015a: Poleward displacement of coastal upwelling-favorable winds in the ocean's eastern boundary currents through the 21st century. *Geophysical Research Letters*, **42** (15), 6424–6431.
- Rykaczewski, R. R., and Coauthors, 2015b: Poleward displacement of coastal upwelling-favorable winds in the ocean's eastern boundary currents through the 21st century. *Geophysical Research Letters*, **42** (15), 6424–6431.
- Salvanes, A. G. V., and Coauthors, 2015: Spatial dynamics of the bearded goby and its key fish predators off n amibia vary with climate and oxygen availability. *Fisheries oceanography*, **24**, 88–101.
- Santos, F., M. Gomez-Gesteira, I. Alvarez, and Coauthors, 2012: Differences in coastal and oceanic sst trends due to the strengthening of coastal upwelling along the benguela current system. *Continental Shelf Research*, **34**, 79–86.
- Schwing, F. B., T. Murphree, P. Green, and Coauthors, 2002: The evolution of oceanic and atmospheric anomalies in the northeast pacific during the el niño and la niña events of 1995–2001. *Progress in Oceanography*, **54** (1-4), 459–491.
- Shannon, L., J. Agenbag, and M. Buys, 1987: Large-and mesoscale features of the angolabenguela front. South African Journal of Marine Science, 5 (1), 11–34.

- Small, R. J., and Coauthors, 2015: The benguela upwelling system: Quantifying the sensitivity to resolution and coastal wind representation in a global climate model. *Journal of Climate*, **28** (**23**), 9409–9432.
- Smith, T. M., and R. W. Reynolds, 2005: A global merged land-air-sea surface temperature reconstruction based on historical observations (1880–1997). *Journal of Climate*, **18** (12), 2021–2036.
- Storto, A., S. Masina, and A. Navarra, 2016: Evaluation of the cmcc eddy-permitting global ocean physical reanalysis system (c-glors, 1982–2012) and its assimilation components. *Quarterly Journal of the Royal Meteorological Society*, **142** (695), 738–758.
- Stuecker, M. F., 2018: Revisiting the pacific meridional mode. *Scientific reports*, 8 (1), 3216.
- Sydeman, W. J., and Coauthors, 2014a: Climate change and wind intensification in coastal upwelling ecosystems. *Science*, **345** (**6192**), 77–80.
- Sydeman, W. J., and Coauthors, 2014b: Multivariate ocean-climate indicators (moci) for the central california current: Environmental change, 1990–2010. *Progress in Oceanog-raphy*, **120**, 352–369.
- Tarazona, J., and W. Arntz, 2001: The peruvian coastal upwelling system. *Coastal Marine Ecosystems of Latin America*, Springer, 229–244.
- Thomas, M. D., A. M. De Boer, H. L. Johnson, and D. P. Stevens, 2014: Spatial and temporal scales of sverdrup balance. *Journal of Physical Oceanography*, **44** (10), 2644–2660.
- Tim, N., E. Zorita, and B. $H\tilde{A}_{4}^{\frac{1}{4}}$ nicke, 2015: Decadal variability and trends of the benguela upwelling system as simulated in a high-resolution ocean simulation. *Ocean Science*, **11** (3), 483–502.
- Toniazzo, T., C. R. Mechoso, L. C. Shaffrey, and J. M. Slingo, 2010: Upper-ocean heat budget and ocean eddy transport in the south-east pacific in a high-resolution coupled model. *Climate dynamics*, **35** (7-8), 1309–1329.
- Tsujino, H., and Coauthors, 2018: Jra-55 based surface dataset for driving ocean-sea-ice models (jra55-do). *Ocean Modelling*.
- Wang, C., and Coauthors, 2012: Multidecadal covariability of north atlantic sea surface temperature, african dust, sahel rainfall, and atlantic hurricanes. *Journal of Climate*, **25** (15), 5404–5415.

- Wang, D., T. C. Gouhier, B. A. Menge, and A. R. Ganguly, 2015: Intensification and spatial homogenization of coastal upwelling under climate change. *Nature*, 518 (7539), 390.
- Wang, M., and Coauthors, 2011: Neuronal basis of age-related working memory decline. *Nature*, **476** (7359), 210.
- Wolter, K., and M. S. Timlin, 2011: El niño/southern oscillation behaviour since 1871 as diagnosed in an extended multivariate enso index (mei. ext). *International Journal of Climatology*, **31** (7), 1074–1087.
- Wooster, W. S., 1963: Eastern boundary currents. The sea, 2, 253–280.
- Xu, Z., P. Chang, I. Richter, and G. Tang, 2014: Diagnosing southeast tropical atlantic sst and ocean circulation biases in the cmip5 ensemble. *Climate dynamics*, **43** (11), 3123–3145.
- Zalesak, S. T., 1979: Fully multidimensional flux-corrected transport algorithms for fluids. Journal of computational physics, **31** (3), 335–362.
- Zheng, Y., and Coauthors, 2010: Upper-ocean processes under the stratus cloud deck in the southeast pacific ocean. *Journal of Physical Oceanography*, **40** (1), 103–120.